

Lagrangian Dynamics in High-Dimensional Point-Vortex Systems

Jeffrey B. Weiss,¹ Antonello Provenzale,² and James C. McWilliams³

Abstract

We study the Lagrangian dynamics of systems of N point vortices and passive particles in a two-dimensional, doubly periodic domain. The probability distribution function of vortex velocity, p_N , has a slow-velocity Gaussian component and a significant high-velocity tail caused by close vortex pairs. In the limit for $N \rightarrow \infty$, p_N tends to a Gaussian. However, the form of the single-vortex velocity causes very slow convergence with N ; for $N \approx 10^6$ the non-Gaussian high-velocity tails still play a significant role. At finite N , the Gaussian component is well modeled by an Ornstein-Uhlenbeck (OU) stochastic process with variance $\sigma_N = \sqrt{N \ln N / 2\pi}$. Considering in detail the case $N = 100$, we show that at short times the velocity autocorrelation is dominated by the Gaussian component and displays an exponential decay with a short Lagrangian decorrelation time. The close pairs have a long correlation time and cause nonergodicity over at least the time of the integration. Due to close vortex dipoles the absolute dispersion differs significantly from the OU prediction, and shows evidence of long-time anomalous dispersion. We discuss the mathematical form of a new stochastic model for the Lagrangian dynamics, consisting of an OU model combined with long-lived close same-sign vortices engaged in rapid rotation and long-lived close dipoles engaged in ballistic motion. From a dynamical-systems perspective this work indicates that systems of dimension $O(100)$ can have behavior which is a combination of both low-dimensional behavior, i.e. close pairs, and extremely high-dimensional behavior described by traditional stochastic processes.

PACS: 47.32.Cc, 47.52.+j, 47.27.Qb

January 22, 1998

to appear in *Physics of Fluids*

¹ PAOS, Campus Box 311, University of Colorado, Boulder, CO 80309-0311, USA, jweiss@colorado.edu.

² JILA, Campus Box 440, University of Colorado, Boulder, CO 80309-0440, USA; permanent address: Istituto di Cosmogeofisica del CNR, C.so Fiume 4, I-10133 Torino, Italy.

³IGPP, UCLA, Los Angeles, CA 90095-1567.

1. Introduction

Advection of passive and active tracers is a crucial component in many geophysical processes: ozone transport in the stratosphere, pollutant dispersal in the atmosphere and the ocean, plankton and salinity transport in the ocean. Additionally, understanding the relationships between Eulerian and Lagrangian statistics is necessary for interpreting data provided by ocean floats and atmospheric balloons.

Standard Lagrangian approaches to transport in fluids are based on the use of either stochastic models or chaotic advection in low-dimensional dynamical systems. Lagrangian stochastic models are generally based on assuming that transport is dominated by unstructured Gaussian random velocity fluctuations, and they are most successful when the system under study has an extremely high-dimensional phase space.^{1, 2} The standard example is Brownian motion which describes the irregular movement of microscopic particles in systems with dimensionality of the order of Avogadro’s number, $O(10^{23})$. In this case, the details of the deterministic description are irrelevant.

Chaotic advection, on the other hand, is based on a fully deterministic description of the phase-space dynamics. It has traditionally been applied to systems with just a few excited degrees of freedom, with very simple spatial structures, and with periodic or quasi-periodic temporal dynamics.^{3, 4, 5} Thus, the traditional application of stochastic models is to highly turbulent flows without strong coherent structures, while low-dimensional chaotic advection is appropriate for flows dominated by a few large-scale waves, vortices, or other structures.^{6, 7}

Geophysical turbulence, however, does not fully belong to either of the above categories. One of the main difficulties encountered in studying Lagrangian advection in geophysical turbulence is, in fact, the complex space-time structure of the flow. The joint effects of

rotation and stratification often induce the presence of energetic coherent structures that contain the majority of the enstrophy of the system.^{8, 9, 10} Intense jets such as the Gulf Stream act as partial barriers to transport, while coherent vortices such as ocean mesoscale eddies and the stratospheric polar vortex can trap particles for long times.^{11, 12, 13, 14, 15} Previous studies of barotropic turbulence have shown that coherent vortices play an important role in the advection of Lagrangian tracers, inducing characteristic signatures that cannot be captured by simple stochastic models.^{12, 16, 17}

In this work, we further explore the properties of advection in flows dominated by strong coherent vortices, and, in particular, we consider an ensemble of many point vortices in two spatial dimensions. Systems of point vortices capture many of the features of two-dimensional turbulent flows.^{18, 19, 20, 21, 22} In geophysically relevant situations the number of energetic coherent structures is neither as large as Avogadro’s number, nor as small as the number of degrees of freedom in simple models of low-dimensional chaotic advection. Systems of N point vortices with $N \sim O(10^m)$, m small, are thus used here as another simplified paradigm: they have an intermediate phase-space dimensionality, and are appropriate for describing advection in vortex dominated flows. As we show below, the dynamics of systems of many point vortices displays properties of both stochastic models and low-dimensional chaotic advection, and provides a useful bridge between high-dimensional stochastic models and low-dimensional chaotic advection.

The remainder of this paper is organized as follows. Section 2 contains an introduction to the dynamics of point vortices, Section 3 addresses the central limit theorem for point-vortex systems and considers the statistical properties of ensembles of point vortices. In Section 4 we discuss the statistical properties of long time-integrations of systems of 100 point vortices, and study the behavior of both the vortices and of passively advected particles. In section 5 we study single-particle dispersion in point-vortex systems and

compare with the dispersion of an ensemble of randomly moving particles described by the Ornstein-Uhlenbeck (OU) stochastic process.² Finally, in Section 6 we present conclusions and perspectives, and discuss a possible alternative stochastic model for describing advection in point-vortex systems.

2. Point-Vortex Dynamics

Point vortices are singular solutions of the Euler equations in two spatial dimensions. The dynamics of an ensemble of point vortices is described self-consistently by a system of equations that take the non-canonical Hamiltonian form

$$\Gamma_i \frac{dx_i}{dt} = \frac{\partial H}{\partial y_i}, \quad \Gamma_i \frac{dy_i}{dt} = -\frac{\partial H}{\partial x_i}, \quad (1)$$

where $\mathbf{x}_i = (x_i, y_i)$ is the position of the i -th vortex with constant circulation Γ_i , H is the Hamiltonian

$$H(\{\mathbf{x}_i\}) = - \sum_{\substack{i,j=1 \\ i \neq j}}^N \frac{\Gamma_i \Gamma_j}{2} G(\mathbf{x}_i, \mathbf{x}_j), \quad (2)$$

N is the number of vortices, and the form of the Green function G depends on the boundary conditions.²³ The positions x_i and y_i play the role of non-canonically conjugate variables, the number of degrees of freedom is equal to the number of vortices, and the dimensionality of the phase space is twice the number of vortices. The number of independent conserved quantities of (1) and (2) also depends on the boundary conditions, but it is always finite and small. Hence, an assembly of more than a few vortices behaves chaotically.

Passively advected particles are easily incorporated in point-vortex systems. A point vortex with zero circulation, $\Gamma_i = 0$, is advected by the other vortices but has no influence on the velocity of any other vortex. Such passively advected particles will be referred to here as *passives*, and particles with $\Gamma_i \neq 0$ as vortices. Recently, the motion of passive particles

in point-vortex systems has been the subject of several investigations.^{16, 24, 25} These studies have shown that point vortices are surrounded by finite-size islands of regular Lagrangian motion, where passives can be trapped for very long times. This implies the existence of long-time non-ergodicity in passive particle motion, where averages over ensembles of different advected particles differ from time averages over single-particle trajectories. In turn, this may lead to long lasting differences between Eulerian and Lagrangian averages and the possibility of non-Brownian (anomalous) dispersion. In the following, we explore in detail some of these issues.

In this work we use periodic boundary conditions because it is the only domain that has the needed properties. A closed domain has a finite maximum separation and is thus not suited to study long-time dispersion properties. This leaves the infinite plane, the periodic plane (2-torus), and the sphere. The infinite plane is unsuitable because motion is not homogeneous with a finite number of vortices. On a sphere, there is no unique way to count the number of times a particle travels around the domain, and thus the sphere does not allow a satisfactory definition of particle dispersion at long times. Thus the only boundary condition which meets our requirements is that of the periodic domain. In addition, most simulations of homogeneous turbulence use these boundary conditions.

The Green function G for point vortices on a periodic domain with length 2π may be written as^{26, 27}

$$G(\mathbf{x}_i, \mathbf{x}_j) = \sum_{m=-\infty}^{\infty} \ln \left(\frac{\cosh(x_i - x_j - 2\pi m) - \cos(y_i - y_j)}{\cosh(2\pi m)} \right) - \frac{(x_i - x_j)^2}{2\pi}. \quad (3)$$

The function G can be shown to be periodic in x and y , and invariant under the transformation $x \rightleftharpoons y$. The velocity of the i -th vortex resulting from (1), (2), and (3) is a sum over the velocities induced by each of the other vortices:

$$\begin{aligned}
 u_i &= \sum_{\substack{j=1 \\ j \neq i}}^N \Gamma_j \sum_{m=-\infty}^{\infty} \frac{-\sin(y_i - y_j)}{\cosh(x_i - x_j - 2\pi m) - \cos(y_i - y_j)}, \\
 v_i &= \sum_{\substack{j=1 \\ j \neq i}}^N \Gamma_j \sum_{m=-\infty}^{\infty} \frac{\sin(x_i - x_j)}{\cosh(y_i - y_j - 2\pi m) - \cos(x_i - x_j)},
 \end{aligned} \tag{4}$$

where $\mathbf{u} = (u_i, v_i) = (dx_i/dt, dy_i/dt)$. The dynamics on the periodic domain has two invariants, the components of the linear momentum, corresponding to translation parallel to the x and y axes; $P_x = \sum_{i=1}^N \Gamma_i y_i$ and $P_y = \sum_{i=1}^N \Gamma_i x_i$. Angular momentum is not an invariant because the periodic boundary conditions break the rotational symmetry. The invariants P_x and P_y are independent only if the total circulation $\sum \Gamma_i$ is zero.²³ In this case, the motion is chaotic for $N > 3$.

3. Point-Vortex Configurations

In this section we discuss the properties of instantaneous configurations of N vortices. We restrict ourselves to configurations with zero total circulation and an equal number of positive and negative vortices.

First consider the velocity induced at a point $\mathbf{x}_0 = (x_0, y_0)$ by a single vortex at \mathbf{x}_1 . In the limit $r = |\mathbf{x}_1 - \mathbf{x}_0| \rightarrow 0$ the velocity (4) asymptotically approaches the velocity generated by a single vortex on the infinite domain, $2\Gamma/r$.^{*} At larger distances from the vortex, the domain periodicity modifies this simple form of the velocity. In practice, the

^{*}Note that with the choice (3) for the Green function, the timescale differs from that usually used on the infinite plane by a factor of 4π ; hence the velocity from a close vortex is here a factor 4π greater than the expression usually used on the infinite domain.²³

velocity on the periodic domain departs significantly from the infinite plane result only for separations greater than approximately one sixth of the domain.

Next, consider the probability density function (pdf) for the velocity resulting from a single vortex, $p_1(\mathbf{u})$. This has been studied in detail by Min et al in the case of the infinite domain.²⁸ If the position of the vortex is chosen at random from a uniform distribution, then the high velocity limit of p_1 is easily calculated. Since the probability of having separation between r and $r + dr$ is $2\pi r dr$, and since for small r the velocity scales as $1/r$ then for large $|\mathbf{u}|$, $p_1(\mathbf{u}) \sim p(r(|\mathbf{u}|)) |dr/d|\mathbf{u}|| \sim 1/|\mathbf{u}|^3$. This scaling for large velocities is independent of the boundary conditions, as the boundaries are irrelevant at sufficiently small separations. The detailed form of the distribution for smaller $|\mathbf{u}|$ does, however, depend on the specific form of \mathbf{u} for a periodic domain, and it depends on the direction of \mathbf{u} as well as its magnitude.

Since we are interested in the dynamics of systems of several point vortices, we now consider the velocity induced at a point by a system of N vortices with $|\Gamma_i| = 1$. This velocity is merely the sum of the velocities due to each vortex separately. If the vortices are randomly placed, then the velocity is the sum of N random numbers, and its pdf $p_N(\mathbf{u})$ is determined by $p_1(\mathbf{u})$. For functions p_1 which decay sufficiently rapidly, the central limit theorem applies and p_N approaches a Gaussian. Most statements of the central limit theorem require that the variance of p_1 be finite. Here, since $p_1 \sim 1/|\mathbf{u}|^3$ the variance $\int |\mathbf{u}|^2 p_1(|\mathbf{u}|) d|\mathbf{u}|$ diverges logarithmically. However, this divergence is sufficiently slow that the central limit theorem still applies and as $N \rightarrow \infty$, p_N does become Gaussian. For more details, see the Appendix, Min et al²⁸, and Ibragimov and Linnik.²⁹

For large but not infinite N , the velocity pdf of an ensemble of vortices displays interesting properties. For distributions with finite variance, the convergence to a Gaussian is quite rapid. For example, if p_1 were constant over a finite region and zero elsewhere,

then p_N is quite close to Gaussian even for $N = 5$. However, for distributions with slowly diverging variance, such as the case here, the convergence to a Gaussian is slow and is called “non-normal”.²⁹ For non-normal convergence, the variance of the sum scales differently than the normal case. In the Appendix we show that for point vortices the variance of the asymptotic Gaussian is $\sigma_N = \sqrt{N \ln N / 2\pi}$. Figure 1 shows how $p_N(u/\sigma_N)$ asymptotically approaches a normal distribution. Due to symmetry, $p_N(u) = p_N(v)$ and these two distributions have been combined into a single pdf. Further, p_N is even and we combine positive and negative velocities. A least-squares fit of the small velocity portion of the distribution to a Gaussian provides a variance of approximately one (as expected for $N \rightarrow \infty$) and an amplitude 0.9 of that of a normal distribution. One sees that even though the central limit theorem formally applies, the convergence is extremely slow and even for large N , p_N has significant high-velocity tails. Further, the small velocity part of p_N is well approximated by a Gaussian with the asymptotic variance, but with amplitude less than one due to the significant fraction of events contained in the high-velocity tails. In what follows, we show that both the Gaussian portion of the pdf at small velocities and the high-velocity tails play an important role in the advection process.

In the remainder of this paper we focus on systems of 100 point vortices. Similar results are obtained with other values of N between about 10 and a thousand. From the perspective of dynamical systems, an ensemble of 100 point vortices has a 200-dimensional phase space; it is thus quite high dimensional. However, it is still reasonable to numerically integrate the equations for significant times. From the perspective of the central limit theorem, due to the slow non-normal convergence, $N = 100$ is not large enough for p_{100} to be completely Gaussian.

We next consider several different initial configurations of the N vortices. The circulations of the vortex populations are characterized by $\bar{\Gamma}$, the average of the absolute

value of the individual circulations. We focus on configurations with $\bar{\Gamma} = 1$, and with random individual circulations uniformly distributed in the range $0.8\bar{\Gamma} \leq |\Gamma_i| \leq 1.2\bar{\Gamma}$. The variation in the individual Γ_i 's is included to break any symmetry in vortex pair interactions that may arise in a system with identical $|\Gamma_i|$'s. For each configuration, the initial vortex positions are randomly chosen in the square domain $[0, 2\pi]^2$. For simplicity we only consider initial conditions with $P_x = P_y = 0$.

The set of initial configurations discussed above can have a range of energies, $E = H(\{\mathbf{x}_i\})/4\pi^2$. Close opposite-sign vortex pairs give a large negative contribution to the energy, while close same-sign pairs provide a positive contribution. Thus, depending on the random initial positions of the vortices, the energy of the system may take different values. In Figure 2 we show the density of states, i.e., the number of states with energy in a given interval, obtained from 10^4 different realizations of the initial vortex configurations described above with $N = 100$. This distribution has a mean of -0.076, a variance of 1.18, and a skewness coefficient of 0.85. In the following we integrate the motion of 300 random configurations extracted from this ensemble for a relatively short time, $T = 0.1$. The two vertical dotted lines indicate two arbitrarily chosen configurations that have been integrated for a much longer time, $T = 30$.

The relationship between vortex speed and nearest neighbor distance for all the 100 vortices in the 300 randomly chosen configurations is seen in Figure 3. Large speeds are associated with close nearest neighbors. From this we may conclude that the high velocities in the tail of the pdfs are due to the presence of a single close vortex and not to the superposition of the contributions of several different vortices. Thus, high-velocity tails in p_{100} are essentially two-vortex phenomena and not many-body effects. This implies that in the limit $N \rightarrow \infty$, as the tails of p_N disappear, the importance of two-vortex interactions goes to zero. However, given the slow convergence of p_N , two-vortex interactions will be

important even for very large N .

4. Long-Time Integrations

In this section we focus on the phase-space trajectories obtained by a relatively long-time integration of the two randomly selected initial configurations indicated in Figure 2. These initial configurations have $N = 100$ vortices and $N_p = 100$ passives. The configurations were integrated until $T = 30$ using a fourth-order Runge-Kutta method with fixed time step $\Delta t = 10^{-5}$. The positions and velocities of the vortices were saved every $\Delta t_s = 10^{-2}$.

The Cartesian velocity pdfs, averaged over time and all vortices, denoted by $\bar{p}(u)$, are obtained by measuring u and v for all vortices every Δt_s throughout the integration; again, from symmetry $\bar{p}(u) = \bar{p}(v) = \bar{p}(-u) = \bar{p}(-v)$ so $\pm u$ and $\pm v$ are combined into a single pdf. The pdfs for the vortex and passive velocities in each of the two solutions are shown in Figure 4. The central part of each pdf, $|u| \lesssim 20$, is well approximated by the same Gaussian which fits the central part of p_{100} ; it has the theoretical asymptotic width $\sigma_{100} = \sqrt{100 \ln 100 / 2\pi} \approx 8.56$ and amplitude 0.9 of a Gaussian with unit normalization. Thus the vortices and passives in the two solutions all have the same small-velocity pdf as each other and as an ensemble of random initial conditions.

The high-velocity tails of \bar{p} for the two solutions are, however, significantly different. One solution has a significant excess over p_{100} at large velocities, while the other has a deficit. Note that both solutions, however, have a deficit at extremely large velocities, $u \gtrsim 250 \approx 30\sigma_{100}$. The pdf with smaller tail in the vortices comes from the same integration as the pdf with the larger tail in the passives, and vice-versa. This is not significant, and is merely the result of picking only two random initial conditions.

The lack of convergence of the pdfs over the time of the integration T indicates that T is not long enough for the system to forget its initial conditions. By other measures, however, T is very long. A typical eddy turnover time, estimated as the time for a vortex at a typical vortex separation $2\pi/\sqrt{N}$ from another vortex to rotate in a complete circle, is approximately 0.4. Another measure of the eddy turnover time is $(\sum \Gamma_i^2)^{1/2} \approx 0.1$. Thus T is $O(100)$ eddy turnover times. A completely different measure of the length of the integration is that in a time of T the particles travel around the basic periodic domain several times. All of this indicates that the correlation time for the tail of the pdf is very long, and that the point-vortex system displays a very long memory with an associated lack of ergodicity over large, if not infinite, time intervals. While this is consistent with what has already been observed for systems of a few point vortices,^{16, 27} it is somewhat surprising that this phenomenon persists in a system with so many degrees of freedom.

A standard statistic for studying velocity time series is the Lagrangian velocity autocorrelation $R(\tau)$,

$$R(\tau) = \frac{\langle \mathbf{u}(t) \cdot \mathbf{u}(t + \tau) \rangle}{\langle |\mathbf{u}(t)|^2 \rangle}, \quad (5)$$

where $\langle \dots \rangle$ represents an average over time and over particles. The autocorrelations from the long phase-space trajectories for the two populations of vortices and passives are shown in Figure 5. As in the pdfs, there is no significant difference between the vortices and passives. After a very short period with steep decay, the autocorrelation of the vortices and passives follows an exponential extremely well. For τ greater than those shown in the Figure, $R(\tau)$ oscillates around zero. The Lagrangian decorrelation time of the phase-space trajectories, T_L , is estimated by fitting $R(\tau) \sim \exp(-\tau/T_L)$ for the period $\tau = 0.02$ to $\tau = 0.2$, giving $T_L = 0.09 \pm 0.01$. A theoretical estimate of the order of magnitude of T_L can easily be obtained by assuming that T_L is the time it takes for a vortex moving at a typical velocity $\sigma_N = \sqrt{N \ln N}/2\pi$ to cross a distance equal to the typical vortex separation $2\pi/\sqrt{N}$; this estimate gives $T_L \sim (2\pi)^{3/2}/N\sqrt{\ln N} \sim 0.07$, quite close to that effectively

observed. Note also that the common method of estimating the Lagrangian integral time scale, $T_I = \int_0^\infty R(\tau)d\tau$, provides misleading results because the very long memory of the system implies that extremely long integration times are needed to reliably calculate T_I .

Individual vortex and passive trajectories, some examples of which are shown in Figure 6, are in general quite complex. The first two panels of Figure 6 show examples of an intermittently fast moving vortex and of a vortex randomly selected from the population of vortices with moderate average speed. The single fast vortex shown in Figure 6(a) comprises 33% of the extreme tail (velocity greater than $10\sigma_{100}$) of the velocity pdf \bar{p} for its integration. Figure 6(c) shows the particle trajectory of a randomly selected passive particle. The particle trajectories of the slow vortex and the passive are qualitatively similar, although the passive does have more tight loops, indicating that at those times it is close to a vortex. The particle trajectory of the fast vortex is qualitatively different than the other two.

The time series of the speed of the fast vortex, Figure 7, shows clear bimodal behavior with the vortex jumping between slow and fast episodes. A time series of the distance to the closest vortex and its identity, Figure 8, shows that episodes of extremely fast motion coincide with the vortex being close to another, oppositely-signed, vortex, i.e., it is a member of a close dipole. These episodes start and end with changes in the identity of the close vortex. Furthermore, the three separate fast episodes are separated by extremely short periods of slow motion where the closest vortex is significantly further away and changes identity rapidly. The ratio of the distance of the second closest vortex to the distance of the closest vortex, Figure 9, demonstrates that the fast episodes are primarily the result of close dipoles. However, note that during the period from $t \approx 22$ to $t \approx 24$ this distance ratio is smaller than during other fast periods (but still larger than during slow periods), and there are small oscillations in the nearest neighbor distance (Figure 8). Analysis of the

individual vortex trajectories shows that during this period the second closest vortex has the same identity and there is thus a temporary three-vortex bound state.

Before closing this section, we note that we have not detected any significant difference between vortex and passive statistics, in the sense that the internal variability in each of these populations is by far larger than any difference between vortices and passives. This is not too surprising if we consider that the contribution of each individual vortex to the total vorticity field is rather small for $N = 100$, and each individual vortex in the collective field of the other vortices behaves similar to a passive. Significant differences do exist, however, in strong two-body interactions: close vortices accelerate each other and may undergo episodes of fast displacement, while passives trapped in the vicinity of a vortex do not influence its motion.

When passives are close to a vortex, they spin with large velocity and create high-velocity components in the pdf. Moreover, passives close to a vortex tend to remain associated with it for very long times, both on the infinite plane¹⁶ and in periodic domains.³⁰ The presence or absence of high-velocity "bumps" in the pdf is thus entirely determined by the initial conditions, i.e., whether or not the system happens to start with close passives. Only by integrating for times much longer than the trapping time is it possible for the time average pdf to converge to the ensemble average pdf, an issue which is related to the possible non-ergodicity of passive particle motion in point vortex systems.¹⁶ At present, it is unclear whether the trapping islands around the vortices have a time-asymptotic nature or disappear at finite (but long) time. Preliminary runs of few-vortex systems³⁰ have shown that the trapping islands exist up to at least $t = 3000$. By comparison, bound states of vortex couples tend to live for much shorter times.

When a passive is close to a vortex, it thus behaves similar to the vortex with which it is linked, with an additional fast rotational component. Whenever the vortex undergoes

a fast displacement due to vortex dipolar coupling, the trapped passive does as well. A detailed theoretical comparison of the long-time displacement statistics of vortices and passives should thus carefully evaluate the probability that a passive be trapped near a vortex (which is related to the initial conditions and determined mainly by geometric factors) and the lifetime of vortex-vortex and vortex-passive couples. On a purely heuristic basis, the present simulations have shown no detectable differences between the gross statistical behavior of vortices and passives, at least on the time scales we have considered.

5. Properties of single-particle dispersion

In this section we study the properties of single-particle dispersion in point-vortex systems. A classic stochastic model for describing the motion of advected particles is the Ornstein-Uhlenbeck (OU) process^{2, 31}

$$d\mathbf{x} = \mathbf{u} dt, \quad d\mathbf{u} = -\frac{\mathbf{u}}{T_L} dt + \frac{\sigma_{ou}}{T_L^{1/2}} d\mathbf{W}, \quad (6)$$

where \mathbf{W} is the Wiener process, and $d\mathbf{W}$ is a Gaussian random increment with $\langle d\mathbf{W} \rangle = 0$ and $\langle dW_\alpha(t) dW_\beta(t') \rangle = 2 \delta_{\alpha,\beta} \delta(t - t') dt$, where $\langle \dots \rangle$ indicates an average over an ensemble of independent realizations, and Greek subscripts indicate vector components.

The OU process is characterized by two parameters: a velocity scale σ_{ou} which determines the variance of the velocity pdf, and a timescale T_L which is the Lagrangian decorrelation time of the exponential velocity autocorrelation $R_{ou}(\tau) = \exp(-\tau/T_L)$. Recently, the OU process has been used to model single-particle dispersion in the atmosphere and the ocean.³²

Here, the OU process is a very natural choice for a stochastic model. As we have already seen, the velocity pdf has a significant Gaussian component, leading us to pick a Gaussian process. Additionally, the Lagrangian velocity autocorrelation has a period of

exponential decay, which leads to the OU process. Furthermore, the two parameters of the OU model have already been determined: $\sigma_{ou} = \sigma_{100} \approx 8.56$ and $T_L = 0.09$. The major failure of the OU process is that it does not capture the high-velocity tails of the vortex pdfs. A trajectory of an OU particle with these parameters is shown in Figure 6(d). The large scale motion is similar to that of a slow vortex or passive, but the small scale motion has more sharp turns instead of small loops.

The OU process may thus give a framework for analyzing the time evolution of the vortex statistics, at least for the slow portion of the vortex population. This is in contrast to the application of the central limit theorem in Section 3, which only refers to single instants in time. To explore similarities and differences with the OU process, relatively short-time integrations, until $T = 0.1$, were performed on 300 initial conditions chosen randomly from those shown in Figure 2. Each initial condition has 100 vortices and 100 passives. This dataset is thus the same size as a single long integration. The velocity pdfs averaged over all initial conditions, as well as the time and initial condition averaged pdfs, are equal to p_{100} .

We now compare the vortex displacements, $\Delta x(\tau) = x(\tau) - x(0)$ with the displacements of the OU process. As is usually done in the study of systems with periodic boundary conditions, we compute displacements from the unfolded trajectories, i.e. by taking into account the number of times a particle has wound around the periodic domain.¹² Again, due to symmetry, we can combine x and y displacements. The OU process has displacements with a Gaussian pdf whose width $\sigma_{\Delta x}$ is

$$\sigma_{\Delta x}^2(\tau) = 2\sigma_{ou}^2 T_L^2 \left(\frac{\tau}{T_L} + e^{-\tau/T_L} - 1 \right). \quad (7)$$

The pdf of vortex displacements at time delay τ can be compared to the OU pdf by scaling each vortex displacement by the above $\sigma_{\Delta x}(\tau)$. The resulting set of pdfs, as obtained by considering all 100 vortices for all 300 initial configurations, are shown in Figure 10 for time delays $\tau = 0.01, 0.02, \dots, 0.09$. This figure shows that for small displacements the pdfs

agree with the OU result. However, there are significant large-displacement tails, which are largest for small times, and decrease as τ increases.

To identify the origin of the large-displacement tails, in Figure 11 we show the displacements at $\tau = 0.05$ versus the nearest neighbor distance, for both same-sign and opposite-sign neighbors. The large displacements are associated with close opposite-sign vortices, i.e. a vortex dipole, while there is no correlation between large displacements and close same-sign vortices. Further, the value of the large displacement is well predicted by the motion of an isolated dipole.

We can conclude that the small displacements are essentially a mean-field process, in that 1) they are due to the action of many other vortices and 2) they are well captured by a stochastic model such as the OU process, which is known to work well for extremely high-dimensional systems such as Brownian motion. On the other hand, the large displacements are essentially due to two-body interactions, namely, temporary coupling of opposite-sign vortices. Same-sign couples rotate rapidly about their center of vorticity, and otherwise behave similarly to a single vortex with larger circulation. Thus, they contribute to the high-velocity tails, but do not contribute to the large-displacement tails. Similar results are observed for the passive particles, with the usual caveat that when passives couple with a vortex they do not affect its velocity, but they can be trapped in the vicinity of a vortex undergoing fast dipolar motion.

We next turn to the temporal evolution of the average vortex and passive displacement, i.e, to absolute or single-particle dispersion. The single-particle dispersion of a system of moving particles is defined as

$$A^2(\tau, t) = \langle (\mathbf{x}(t + \tau) - \mathbf{x}(t))^2 \rangle_p, \quad (8)$$

where $\langle \dots \rangle_p$ indicates an average over the ensemble of particles. When the particle motion is statistically stationary, as is the case here, A^2 becomes independent of t . The finite-time

dispersion coefficient is defined as $D(\tau) = A^2/2\tau$. For motions in differentiable velocity fields, the short time dispersion is ballistic, i.e. $A^2(\tau) \propto \tau^2$ for $\tau \ll T_I$ where T_I is the Lagrangian integral time scale, defined as the integral of the velocity autocorrelation. If T_I is finite, then at large times the dispersion becomes Brownian-like, i.e. $A^2(\tau) \sim \tau$. The usual dispersion coefficient is thus defined in the infinite time limit, $D = \lim_{\tau \rightarrow \infty} D(\tau)$.

For the OU process, the appropriate ensemble of particles is a collection of independent realizations of the Wiener process. The diffusion coefficient then becomes

$$D_{ou}(\tau) = 2\sigma_{ou}^2 T_L \left[1 - \frac{T_L (1 - e^{-\tau/T_L})}{\tau} \right], \quad (9)$$

which has the infinite time limit $D_{ou} = 2\sigma_{ou}^2 T_L$.

For the point-vortex system, the appropriate ensemble in Equation (8) is the collection of vortices or passives at a single time in a single integration. As for displacements, dispersion is calculated using unfolded trajectories. The four resulting diffusion coefficients are shown in Figure 12. There is no significant difference between the vortices and passives, and thus the best estimate is obtained by averaging the four diffusion coefficients. The diffusion coefficient for the OU process, Equation (9), is shown for comparison. Also shown is the expected error of the mean for four ensembles of 100 OU particles, which is calculated with standard statistical methods. For short times, $t \lesssim 0.1 \sim T_L$, the OU process captures the dispersion reasonably well. For intermediate times, $T_L \lesssim t \lesssim 2 \sim 20T_L$, the OU process overestimates the dispersion. For long times, $t \gtrsim 20T_L$, the diffusion coefficient appears to grow beyond that of the OU prediction. This anomalously large single-particle dispersion is presumably due to the tails in the velocity pdfs and large displacements of long-lived close dipoles. It is an interesting question, which remains unanswered at the moment, whether the single-particle dispersion becomes Brownian at very large times in point-vortex systems.

6. Conclusions

In this paper we analyze the Lagrangian dynamics of vortices and passives in high-dimensional, $N = O(100)$, point-vortex systems. We find that the behavior can be understood by partitioning the system into two components: (1) mean-field behavior resulting from the collection of distant vortices, and (2) high-velocity behavior resulting from close pairs (and, occasionally, triplets or more).

The partition in the statistical dynamics is due to the slow, non-normal convergence of p_N . In the limit $N \rightarrow \infty$ the velocity pdf is Gaussian and only mean-field behavior occurs. The mean-field behavior is well modeled as an Ornstein-Uhlenbeck (OU) stochastic process. This part of the dynamics has a short correlation time, $T_L = 0.09$, which can be estimated by simple arguments based on the turn-over times for average vortex separation. However, due to the $1/|\mathbf{u}|^3$ behavior of the velocity pdf for a single vortex at large $|\mathbf{u}|$, the convergence to the Gaussian implied by the central limit theorem is extremely slow with N , and the variance of the Gaussian component scales as $\sqrt{N \ln N}$ rather than the more common \sqrt{N} .

The slow convergence is important for physically relevant, large but finite, values of N , where there is a significant, non-Gaussian, high-velocity tail in the pdf. This high-velocity tail has a very long correlation time. Close pairs typically last for much longer than T_L ; indeed, they can last so long that even our longest integrations, of $O(300T_L)$, do not yield reliable statistics for the distribution of pair lifetimes. These long-lived pairs exhibit nonergodic behavior for at least the time of our simulations, which is consistent with previous evidence for long-time nonergodicity with only a few point vortices.^{16, 27}

As a result of the high-velocity tails, the OU process does not accurately capture the single-particle dispersion and the pdf of particle displacements. The small displacements

scale approximately as in the OU model, but the large displacements show no such scaling due to close dipoles. At very short times, of course, the displacements exhibit ballistic scaling, with $D(\tau) \propto \tau$. After the first significant loss of velocity correlation, at $t \sim O(T_L)$, the OU model captures the average dispersion reasonably well. At later times, $t \approx 1 - 5$, the OU model overestimates the single-particle dispersion, and at very large times, $t > 20$, the OU model appears to underestimate the dispersion. This suggests that the diffusion coefficient may continue to increase resulting in long-time anomalous dispersion, rather than saturate as in the OU model around a time of $O(10T_L)$.

It may be possible to construct a new stochastic process that includes both the Gaussian slow vortices and the long-lived, close, high-velocity pairs. The slow vortices would be modeled as an OU process. Since the close same-sign pairs rotate in place, these vortices should be modeled by a process that has negative velocity correlations at very short times. The close dipoles travel large distances, and could be modeled by a Lévy walk.³³ In previous studies of point vortices, Viccelli found anomalous relative dispersion at short times, which he explained as Lévy walks.^{34, 35}

In order to create a combined stochastic process one would need information about the close-pair dynamics. This information could be condensed into two joint pdfs and two scalar probabilities: the joint pdfs of close-pair velocities and lifetimes, separately for the dipoles and same-sign pairs, and the transition probabilities for switching from OU motion to close dipoles and same-sign pairs, i.e., the probabilities for close-pair formation. We already know that the pdf for close pair velocities, which is related to the joint pdf by integrating over lifetime, scales as u^{-3} for large u . If we are only concerned with displacements, then the same-sign pairs can probably be absorbed into the OU component, since their center of vorticity moves as a single vortex. If we wish to model the velocities, however, then the fast rotation of the same-sign pairs is important.

With this information one could construct a stochastic algorithm in which particles move with OU random walks, and, at particular instants, have some probability of becoming members of a dipole or same-sign pair. Once a member of a dipole, the particle moves for some time at a constant velocity in a random direction, with the time and velocity chosen from the joint pdf. Once a member of a same-sign pair, the particle has a high oscillating velocity for some time, plus a slower OU random-walk velocity, again with the time and velocity chosen from the joint pdf. Because of the long correlation time of the close pairs, obtaining a good estimate of these joint pdfs would require significantly longer integrations than we have done here; therefore, we will not propose here an explicit form for the new stochastic model.

How relevant is the range of N we study here for geophysical flows? The number of coherent vortices is not well known in nature, since they are often hard to detect by conventional measurement techniques; for example, the vorticity or potential vorticity fields are usually poorly sampled. However, we can estimate an upper bound on the number of coherent vortices in the large-scale geostrophic regimes of the atmosphere and ocean as the ratio of total area to a typical vortex area, neglecting any stacking in the vertical. (We do not consider the ageostrophic, smaller-scale regimes, for which 2D vortex dynamics are probably less relevant.) A typical geostrophic vortex size is given by the Rossby radius of deformation, which, at midlatitudes, is approximately 30 km in the ocean, and 1000 km in the atmosphere.³⁶ The total areas of the ocean and atmosphere are about 3.5×10^8 km² and 5×10^8 km², respectively. Thus, if the area were filled with closely packed vortices, which is certainly not the case, the ocean would have $O(10^5)$ vortices and the atmosphere would have only $O(10^2)$ vortices. From Figure 1 we see that with this upper bound even the ocean would not be in the infinite N regime and the tails of the pdf would be important. Thus, the behavior described in this paper is representative of what we expect from the number of coherent vortices in the atmosphere and ocean.

The point-vortex system is only an approximation to the dynamics of coherent vortices in geophysical flows. True coherent vortices have a finite core size and a finite lifetime, even though the former is often small and the latter large compared to many geophysical phenomena. The existence of a finite core does not significantly affect the dynamics of passive tracers, as shown by simulations of two-dimensional turbulence.^{12, 16, 17} Since extended coherent vortices effectively retain the matter in and near their cores and can travel long distances over their long lifetimes, they can have considerable influence over large-scale material transports, similarly to what happens for point vortices. On the other hand, the dynamics of the vortices themselves may be affected by the presence of a finite core. In particular, same-sign vortices can merge, a process which is not included in point-vortex dynamics. Although a full answer to the impact of finite cores can only come from simulations of extended vortices, we note that many of the specific Lagrangian properties discussed here are mainly determined by the behavior of close dipoles. These still exist, with similar properties, in the case of extended vortices, suggesting that the results found here for point vortices which are due to dipoles may be more general. Future studies will address the properties of Lagrangian transport in systems of coherent vortices with extended cores and in punctuated point vortex dynamics where instantaneous merger is allowed.

In this paper we have demonstrated several differences of vortex systems from random walking. On the other hand, aspects of the overall dispersion behavior seen in Figure 12 are grossly captured by simple OU diffusion on times very large compared to T_L . Thus, we see this study as giving some further degree of support for the common practice of parameterizing large-scale transports as eddy diffusion. In this context, the eddy diffusion coefficient is a function of the coherent vortex population obtained from Equation (9) with σ_{ou} replaced by σ_N , $D = NT_L \ln N/\pi$. Thus, one may be able to obtain a time-varying eddy diffusion by observing how the vortex population changes over time. However, it may

eventually turn out that the quantitatively significant differences between vortex dispersion and stochastic diffusion imply a significant qualitative difference as well. For example, if the diffusion coefficient continues to grow with time, then for times much longer than these simulations, eddy diffusion will fail.

7. Acknowledgments

The numerical computations of this work have been carried on at the computing center of the Istituto di Cosmogeofisica, Torino, Italy, and at the Laboratory for Computational Dynamics of JILA, University of Colorado, Boulder. JW is partially supported by NSF ECS-9217394 and DOC NA56GP0230. AP is grateful to JILA for support and hospitality during the final part of this work. Support from the EC contract EV5V-CT94-0503 is gratefully acknowledged.

A. Appendix: The Central Limit Theorem for Point Vortices

In this appendix we show that in the limit $N \rightarrow \infty$ the velocity probability density function (pdf) for the velocity due to N randomly placed vortices, p_N , becomes Gaussian with variance $\sigma_N = \sqrt{N \ln N / 2\pi}$. The calculation is based on theorems regarding random variables.²⁹ The fact that p_N becomes Gaussian was mentioned previously by Min, et al;²⁸ the value of the variance is, to our knowledge, new.

The relevant theorems discuss the behavior of z_N , the sum of N independent identically distributed random variables x_i with pdf $F(x)$, scaled by a factor σ_N :

$$z_N = \frac{x_1 + \dots + x_N}{\sigma_N}. \tag{A1}$$

If in the limit $N \rightarrow \infty$ the pdf for z_N converges weakly to some distribution G , then F is said to be in the domain of attraction of G . The family of distributions which have non-empty domains of attraction are called Lévy distributions and are identified by an index α , $0 < \alpha \leq 2$; $\alpha = 2$ corresponds to the normal distribution, and $\alpha = 1$ is the Cauchy distribution.^{29, 33} Here we shall only be concerned with $\alpha = 2$.

Ibragimov and Linnik²⁹ prove that F belongs to the domain of attraction of the normal distribution if and only if the truncated second moment

$$I(X) = \int_{-X}^X x^2 F(x) dx \quad (\text{A2})$$

is slowly varying in the sense that

$$\lim_{X \rightarrow \infty} \frac{I(tX)}{I(X)} = 1 \quad (\text{A3})$$

for all t . They further show that the scaling of the sum, σ_N , is given by the requirement that

$$\lim_{N \rightarrow \infty} \frac{NI(\epsilon\sigma_N)}{\sigma_N^2} = 1, \quad (\text{A4})$$

for some $\epsilon > 0$. As written, Equation (A4) assumes that F has zero mean which is the case of interest here; if F has nonzero mean then another term is needed in the equation.

Here, $p_1(u)$ takes the role of $F(x)$, where $p_1(u)$ is the pdf for the x -component of the velocity, u , produced at the origin from a point vortex with unit circulation placed at a random position in the periodic domain $[-\pi, \pi]^2$. Since the velocity is a vector $\mathbf{u} = (u, v)$ described by a joint distribution $p(u, v)$, p_1 is obtained from

$$p_1(u) = \int_{-\infty}^{\infty} p(u, v) dv. \quad (\text{A5})$$

Due to symmetry the pdfs for u and v are identical and we need only consider one of them. It is sufficient to only consider vortices with positive circulation since changing the sign of

the circulation is equivalent to changing the sign of \mathbf{x} . Thus, allowing random positive and negative unit circulations would not affect p_1 or p_N .

We are interested in the velocity component u due to N vortices, with pdf $p_N(u)$, where u is the unscaled sum of the velocity components of the individual vortices. Thus, if the sum scaled by σ_N has a normal distribution, then p_N is Gaussian with variance σ_N .

While the joint distribution $p(u, v)$ is rather difficult to determine in detail, changing variables allows us to easily integrate over the distribution. The random velocity \mathbf{u} is due to a vortex at a random position \mathbf{x} , so $p(u, v) du dv = p(x, y) dx dy$. Further, since the vortex is placed randomly from a uniform distribution, $p(x, y) = 1/4\pi^2$. A final change of variables to polar coordinates (r, θ) gives

$$\begin{aligned} I(X) &= \int_{-X}^X du \int_{-\infty}^{\infty} dv u^2 p(u, v), \\ &= \frac{1}{4\pi^2} \int d\theta \int dr r u^2(r, \theta). \end{aligned} \tag{A6}$$

To determine the bounds of the integral we need the curve $r(\theta, X)$ such that $u(r, \theta) = X$, with v arbitrary. Since we are interested in the behavior of $I(X)$ in the limit of large X we can use the asymptotic form of Equation (4), $u(r, \theta) = 2 \sin \theta / r$. Since the original integral is over $|u| < X$, in polar coordinates the integration is over $r > 2 \sin \theta / X$; this corresponds to integrating over all points outside two circles with radius $1/X$ centered at $\pm 1/X$. Along the x -axis, $\theta = 0$ or π , r is allowed to go to zero; thus, $v = 2 \cos \theta / r$ can reach both $\pm\infty$ and $r > 2 \sin \theta / X$ does not restrict v . Defining $R(\theta)$ to be the distance from the origin to the edge of the periodic domain results in

$$I(X) = \frac{1}{4\pi^2} \int_0^{2\pi} d\theta \int_{2 \sin \theta / X}^{R(\theta)} dr r u^2(r, \theta). \tag{A7}$$

Despite the fact that the integral covers small u , the limiting behavior of I only

depends on the asymptotic form of $u(r, \theta)$. Writing the velocity as

$$u(r, \theta) = \frac{2 \sin \theta}{r} + g(r, \theta), \quad (\text{A8})$$

where, from Equation (4), $g \sim O(r)$ for small r , gives

$$I(X) = \frac{1}{\pi} \ln X + O(1). \quad (\text{A9})$$

It is now straightforward to verify that $I(X)$ is slowly varying in the sense of (A3), and thus p_1 is in the domain of attraction of the normal distribution. Further, the requirement (A4) is satisfied by

$$\sigma_N = \sqrt{\frac{N \ln N}{2\pi}}. \quad (\text{A10})$$

Thus, in the limit $N \rightarrow \infty$, p_N is Gaussian with variance σ_N . Because this result only depends on the explicit form of u for small separations, it is independent of boundary conditions.

REFERENCES

1. *Stochastic Modelling in Physical Oceanography*, R.J. Adler, P. Müller, R.B. Rozovskii, eds., (Birkhäuser, Boston, 1996).
2. *Selected papers on noise and stochastic processes*, N. Wax, ed., (Dover, New York, 1954).
3. J.M. Ottino, *The kinematics of mixing: stretching, chaos, and transport*, (Cambridge University Press, Cambridge, 1989).
4. *Chaotic Advection, Tracer Dynamics, and Turbulent Dispersion*, A. Babiano, A. Provenzale, A. Vulpiani, eds., *Physica D*, **76**, 1, (1994).
5. *Chaos Applied to Fluid Mixing*, H. Aref and M.S. El Naschie, eds., *Chaos Solitons and Fractals*, **4**, 745, (1994).
6. J.B. Weiss, “Transport and Mixing in Traveling Waves,” *Phys. Fluids A*, **3**, 1379, (1991).
7. J.B. Weiss, “Hamiltonian Maps and Transport in Structured Fluids,” *Physica D*, **76**, 230, (1994).
8. J.C. McWilliams, J.B. Weiss, and I. Yavneh, “Anisotropy and Coherent Vortex Structures in Planetary Turbulence,” *Science*, **264**, 410, (1994).
9. J.C. McWilliams and J.B. Weiss, “Anisotropic Geophysical Vortices,” *CHAOS*, **4**, 305, (1994).
10. *Turbulence and coherent structures*, O. Metais and M. Lesieur, eds., (Kluwer, Dordrecht, 1991).
11. T. Song, T. Rossby, and E. Carter, “Lagrangian studies of fluid exchange between the Gulf Stream and surrounding waters,” *J. Phys. Ocean.*, **25**, 46, (1995).

12. D. Elhmaidi, A. Provenzale, and A. Babiano, “Elementary topology of two-dimensional turbulence from a Lagrangian viewpoint and single-particle dispersion,” *J. Fluid Mech.*, **257**, 533, (1993).
13. R.M. Samelson, “Fluid exchange across a meandering jet,” *J. Phys. Ocean.*, **22**, 431, (1992).
14. J.C. McWilliams, “Submesoscale, coherent vortices in the ocean,” *Rev. Geophys.*, **23**, 165, (1985).
15. F. Paparella, A. Babiano, C. Basdevant, A. Provenzale, and P. Tanga “A Lagrangian Study of the Antarctic Polar Vortex,” *J. Geophys. Res.*, **102 D**, 6765-6773, (1997).
16. A. Babiano, G. Boffetta, A. Provenzale, and A. Vulpiani, “Chaotic advection in point vortex models and two-dimensional turbulence,” *Phys. Fluids*, **6**, 2465, (1994).
17. A. Provenzale, A. Babiano, and A. Zanella, “Dynamics of Lagrangian tracers in barotropic turbulence,” in *Mixing: Chaos and Turbulence*, Proceedings of a NATO Advanced Study Institute, Cargese, Corsica, July 7-20, 1996, in press.
18. J.B. Weiss, “Punctuated Hamiltonian Models of Structured Turbulence,” in *Proceedings of the Centre de Recherche en Mathematiques Workshop on Semi-analytic methods for the Navier-Stokes equations*, K. Coughlin, ed., to appear.
19. G. Riccardi, R. Piva, and R. Benzi, “A physical model for merging in two-dimensional decaying turbulence,” *Phys. Fluids*, **7**, 3091, (1995).
20. J.B. Weiss and J.C. McWilliams, “Temporal Scaling Behavior of Decaying Two-Dimensional Turbulence,” *Physics of Fluids A*, **5**, 608, (1993).
21. R. Benzi, M. Colella, M. Briscolini, and P. Santangelo, “A simple point vortex model for two-dimensional decaying turbulence,” *Phys. Fluids A*, **4**, 1036, (1992).

22. G.F. Carnevale, J.C. McWilliams, Y. Pomeau, J.B. Weiss, and W.R. Young, “Evolution of Vortex Statistics in Two-Dimensional Turbulence,” *Phys. Rev. Lett.*, **66**, 2735, (1991).
23. H. Aref, “Integrable, chaotic, and turbulent vortex motion in two-dimensional flows,” *Ann. Rev. Fluid Mech.*, **15**, 534, (1983).
24. G. Boffetta, A. Celani, and P. Franzese, “Trapping of passive tracers in a point vortex system,” *J. Phys. A*, **29**, 3749, (1996).
25. A. Pentek, T. Tel, and T. Toroczkai, “Chaotic advection in the velocity field of leapfrogging vortex pairs,” *J. Phys. A*, **28**, 2191, (1995).
26. L.J. Campbell, M.M. Doria, and J.B. Kadtko, “Energy of infinite vortex lattices,” *Phys. Rev. A*, **39**, 5436, (1989).
27. J.B. Weiss and J.C. McWilliams, “Nonergodicity of Point Vortices,” *Phys. Fluids A*, **3**, 835, (1991).
28. I.A. Min, I. Mezic, and A. Leonard, “Levy stable distributions for velocity and velocity difference in systems of vortex elements,” *Phys. Fluids*, **8**, 1169, (1996).
29. I.A. Ibragimov, and Yu.V. Linnik, *Independent and Stationary Sequences of Random Variables*, (Wolters-Noordhoff, Groningen, 1971).
30. E. Carena, A. Provenzale, and J. B. Weiss “Eulerian and Lagrangian statistics in point-vortex systems,” in preparation, (1998).
31. H. van Dop, F.T.M. Nieuwstadt, and J.C.R. Hunt, “Random walk models for particle displacements in inhomogeneous unsteady turbulent flows,” *Phys. Fluids*, **28**, 1639, (1985).

32. A. Griffa, “Applications of stochastic particle models to oceanographic problems,” in *Stochastic Modelling in Physical Oceanography*, R.J. Adler, P. Müller, R.B. Rozovskii, eds., (Birkhäuser, Boston, 1996).
33. *Lévy Flights and Related Topics in Physics*, M.F. Shlesinger, G.M. Zaslavsky, and U. Frisch, eds., (Springer-Verlag, Berlin, 1995).
34. J.A. Vieceili, “Dynamics of two-dimensional turbulence,” *Phys. Fluids A*, **2**, 2036, (1990).
35. J.A. Vieceili, “Statistical mechanics and correlation properties of a rotating two-dimensional flow of like-sign vortices,” *Phys. Fluids A*, **5**, 2484, (1993).
36. A.E. Gill, *Atmosphere-Ocean Dynamics*, (Academic Press, San Diego, 1982).

Figure Captions

Figure 1. Probability density function $p_N(u/\sigma_N)$ for the instantaneous velocity u produced by N randomly placed vortices, scaled by $\sigma_N = \sqrt{N \ln N/2\pi}$. Solid lines are p_N for $N = 10^2, 10^4$, and 10^6 . Dashed line is a Gaussian pdf with unit variance and amplitude 0.9. The inset shows same curves on log-log axes, along with the dotted line $\sim 1/u^3$.

Figure 2. Density of states as a function of energy for 10^4 random configurations of 100 vortices. Dashed lines indicate two arbitrary initial condition used for long integrations.

Figure 3. Scatter-plot of instantaneous vortex speed versus nearest neighbor distance for all vortices in 300 randomly chosen configurations. The dashed lines indicate the speed induced by a single vortex with the smallest and largest circulations in the population.

Figure 4. The velocity pdf averaged over time and particles, $\bar{p}(u)$, for a) the vortices, and b) the passives. In each panel, the two solid lines are $\bar{p}(u)$ for the two long integrations discussed in the text, the dotted line is a Gaussian with variance σ_{100} and amplitude 0.9 and the dashed line is $p_{100}(u)$, as in Figure 1, but with the same sample size as \bar{p} .

Figure 5. Velocity autocorrelation function $R(\tau)$, Equation (5), for the two long integrations. Solid lines are the vortices, dashed lines are the passives. The dotted line is the exponential which best fits the average of the vortices and passives, and has a decay time of $T_L = 0.09$.

Figure 6. Individual particle trajectories from the long integrations: a) a fast vortex, where the period of fast motion, $|\mathbf{u}| > 70$, is shown in bold, b) a slow vortex, c) a slow passive, and d) a stochastic particle governed by the Ornstein-Uhlenbeck process, Equation (6). The trajectory of the fast vortex appears not to be smooth because of the finite plotting interval, Δt_s .

Figure 7. Time series for the speed of the fast vortex shown in Figure 6(a).

Figure 8. Nearest neighbor distance for the fast vortex shown in Figure 6(a) (lower curve). The identity of the nearest neighbor is shown in the upper curve: a line at 1.3 indicates a same-sign nearest neighbor, a line at 1.1 indicates an opposite-sign nearest neighbor, and the line jumps to 1.2 every time the identity of the nearest neighbor changes.

Figure 9. Ratio of the distances from the fast vortex shown in Figure 6(a) to its second and first nearest neighbors.

Figure 10. Probability density function of displacements $\Delta x(\tau)$ scaled by the OU expected displacement $\sigma_{\Delta x}$, Equation (7), for $\tau = 0.1, 0.2, \dots, 0.9$, from the 300 short integrations. The dashed line is the OU Gaussian. The inset shows the tails for $\tau = 0.1$ (upper solid curve) and 0.9 (lower solid curve).

Figure 11. Scatter-plot of displacement $\Delta x(\tau)$, $\tau = 0.05$, versus average nearest neighbor distance over the time period for a) opposite-sign pairs, and b) same-sign pairs in the 300 short integrations. The solid line in a) is the displacement of a single dipole on the infinite plane with $|\Gamma| = 1$.

Figure 12. Diffusion coefficient $D(\tau)$ from the two long integrations for the vortices (thin solid curves), passives (thin dashed curves), and the average of the four (thick solid curve). Also shown is the OU diffusion coefficient (thick solid smooth curve) and the envelope of expected error for four ensembles of 100 OU particles (thick dashed curves). The inset shows the same curves for short times.

Figure 1

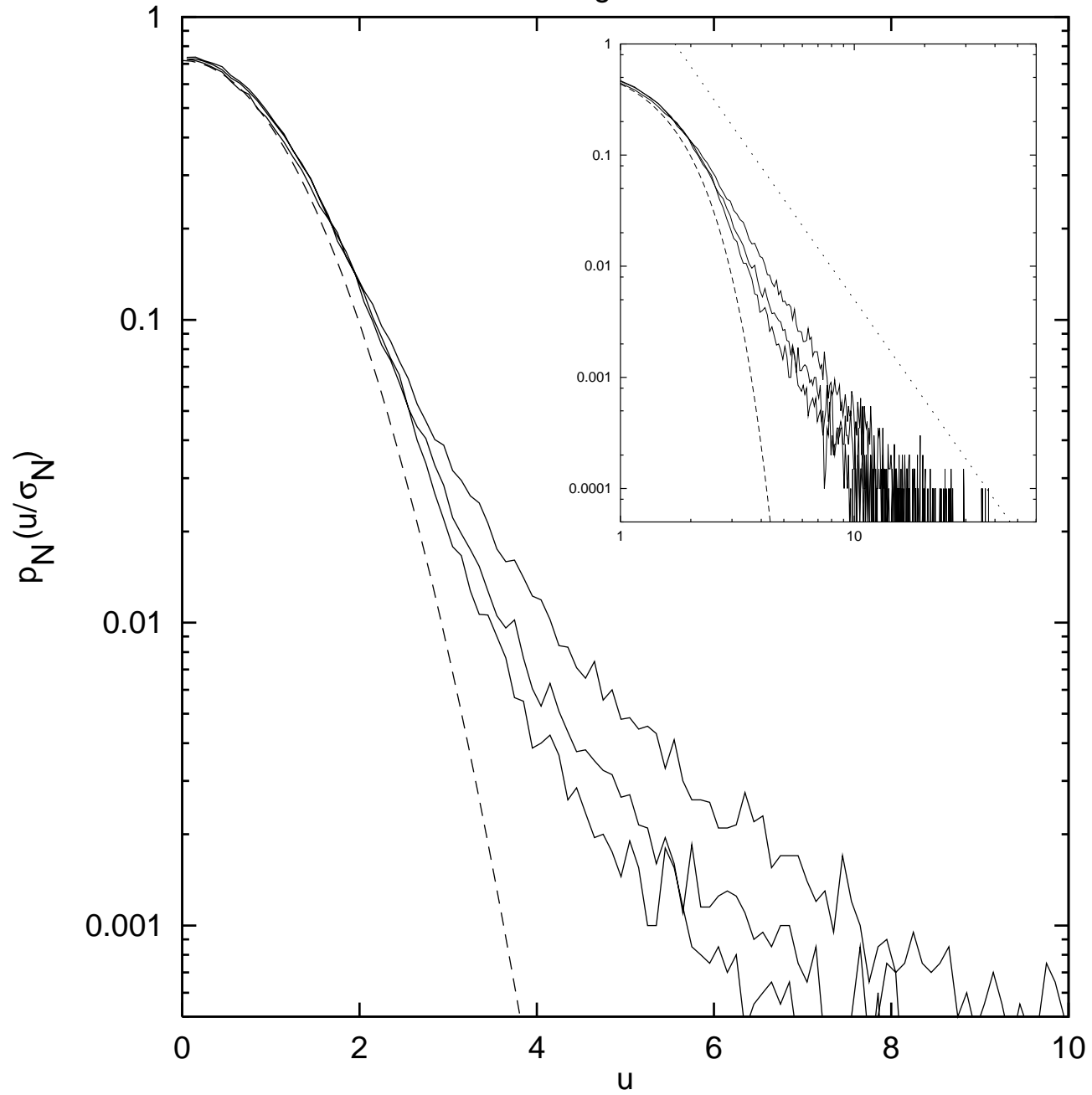


Figure 2

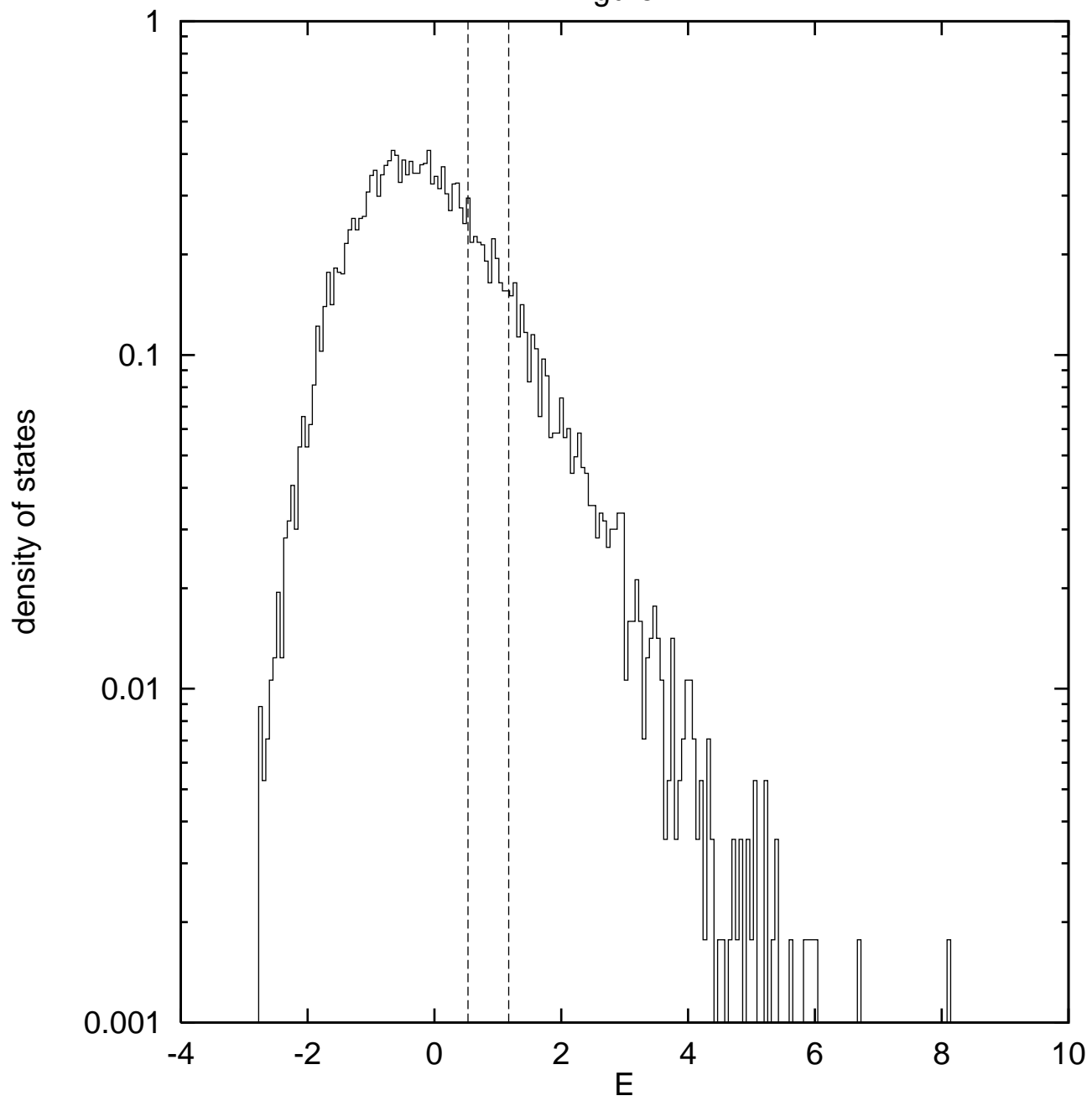


Figure 3

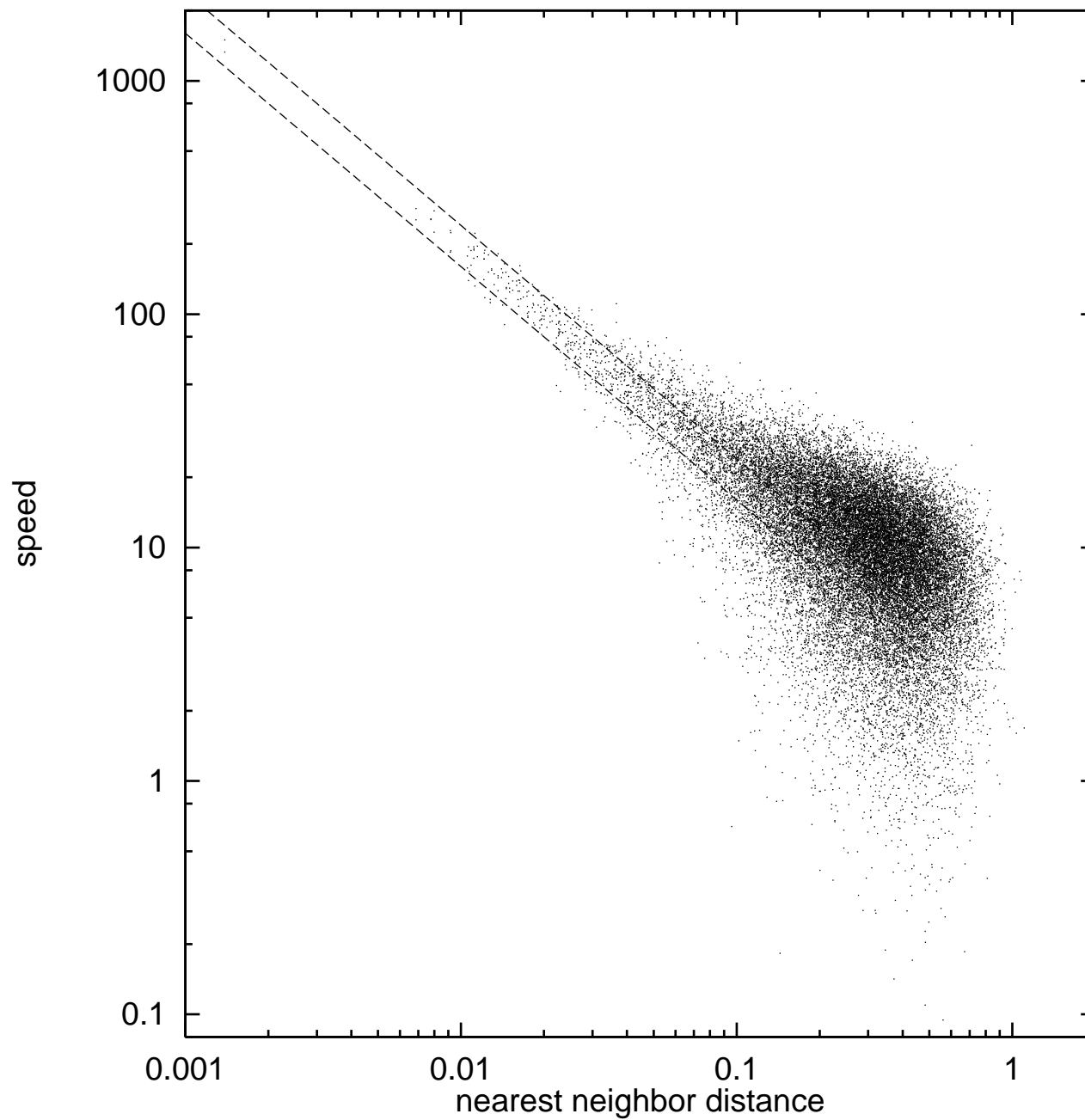


Figure 4(a)

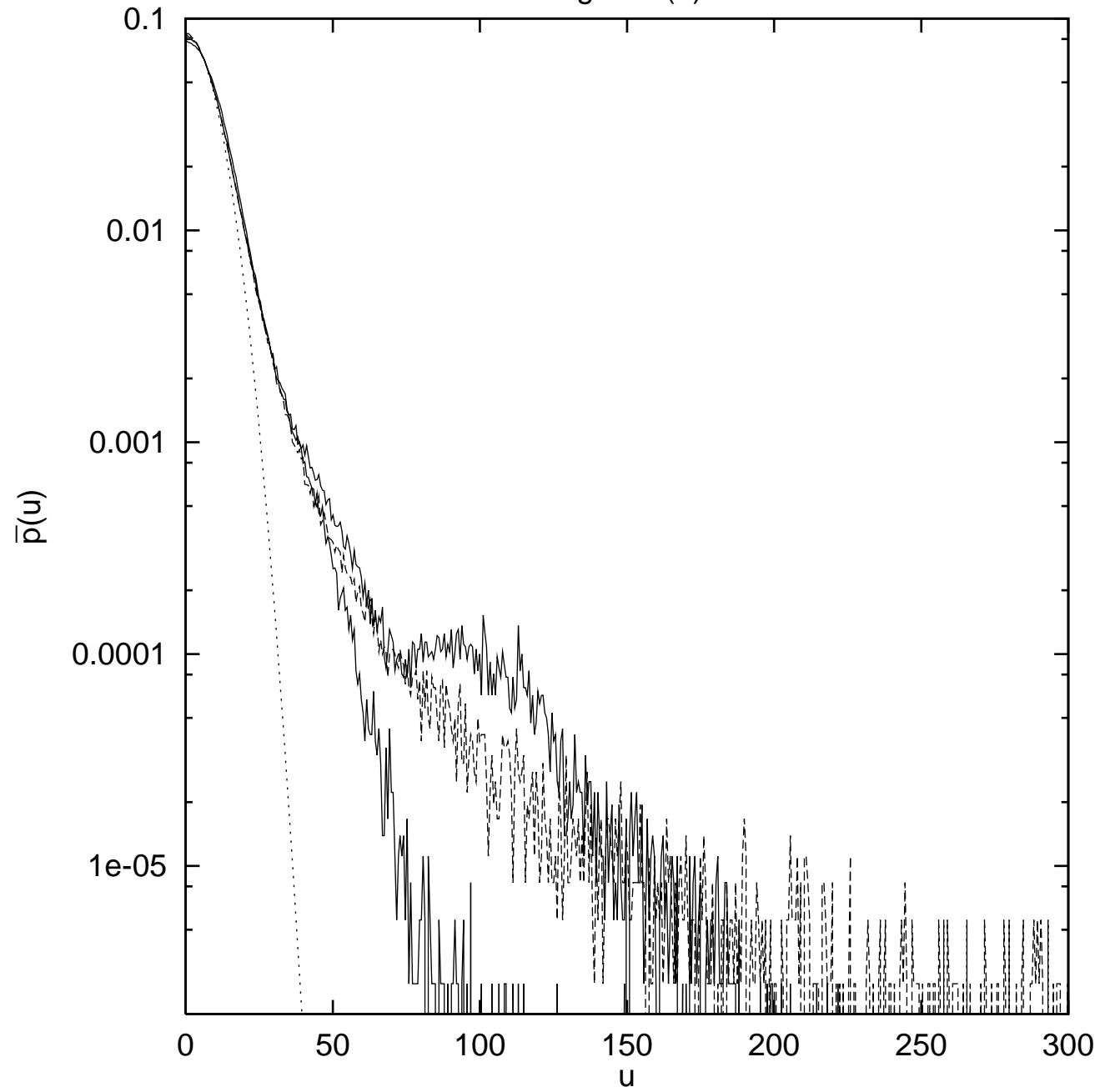


Figure 4(b)

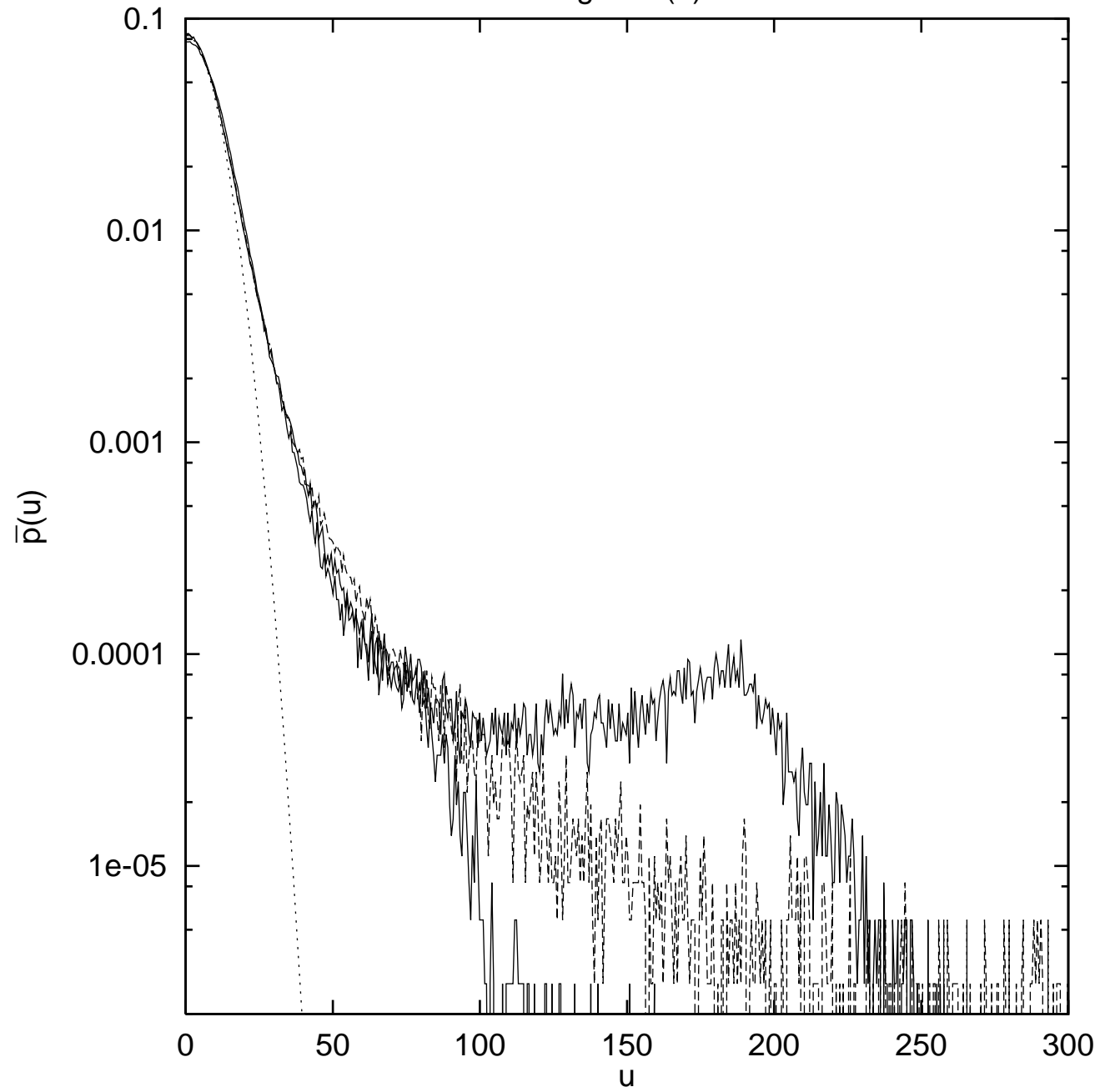


Figure 5

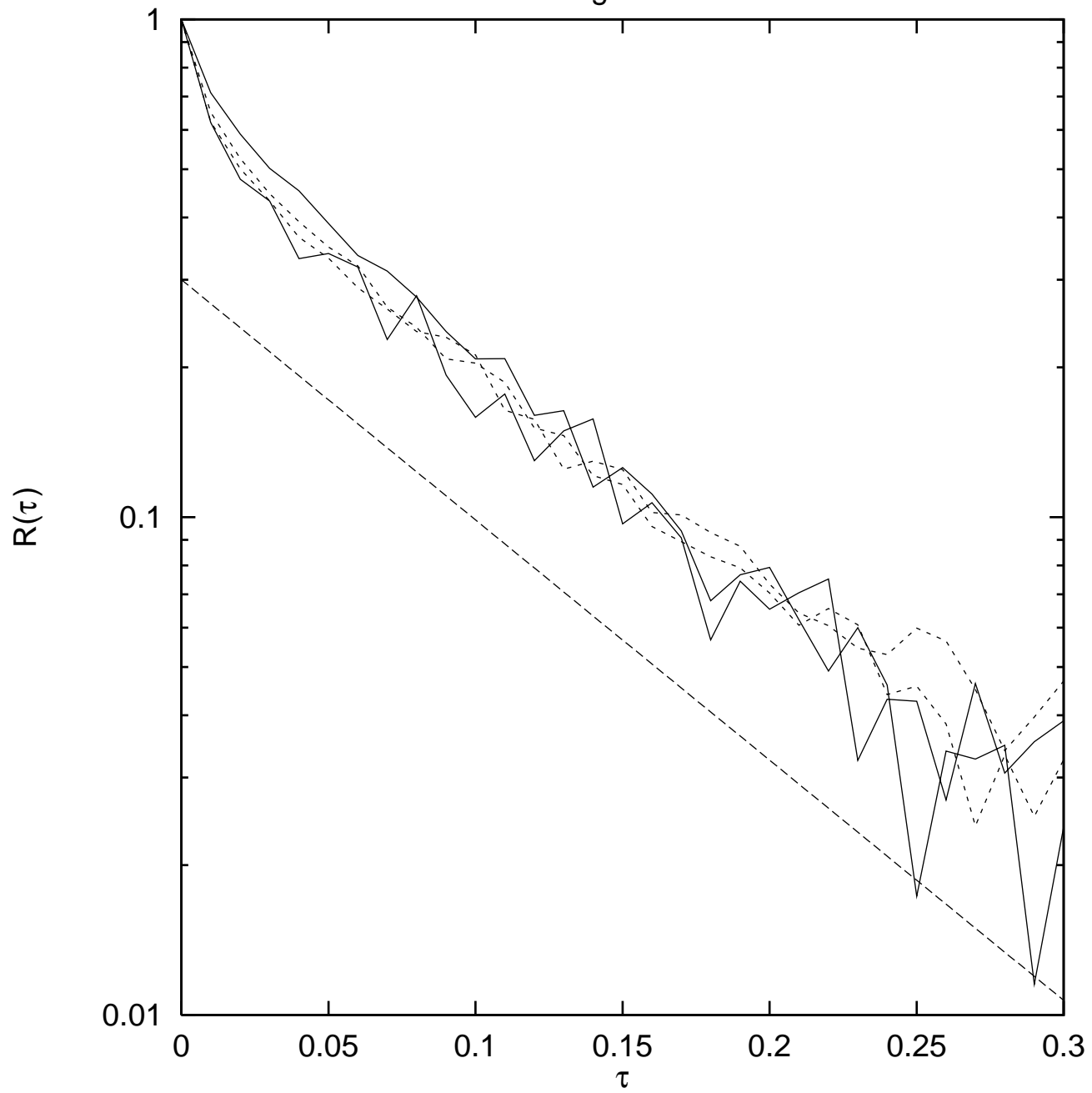


Figure 6(a)

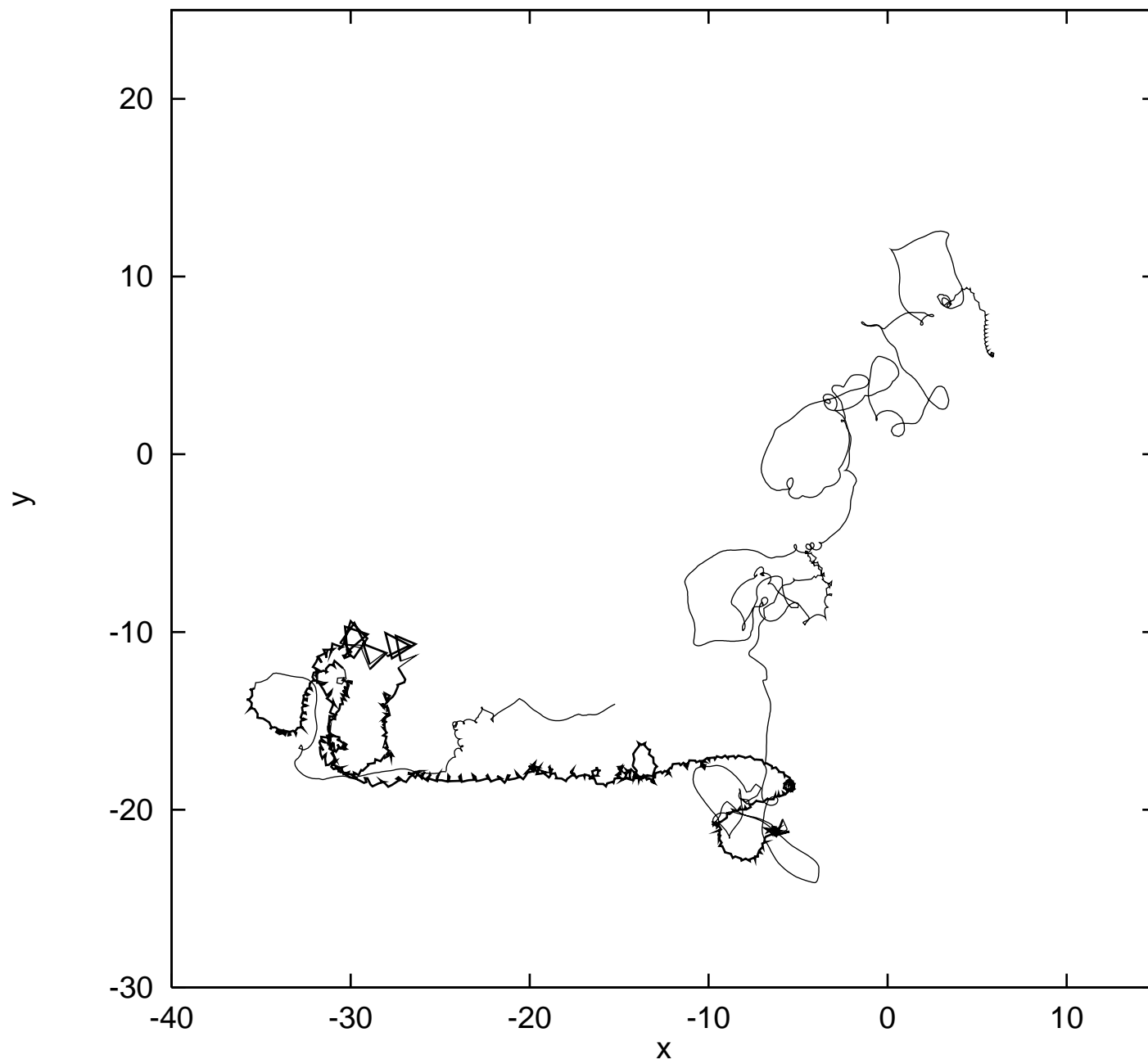


Figure 6(b)

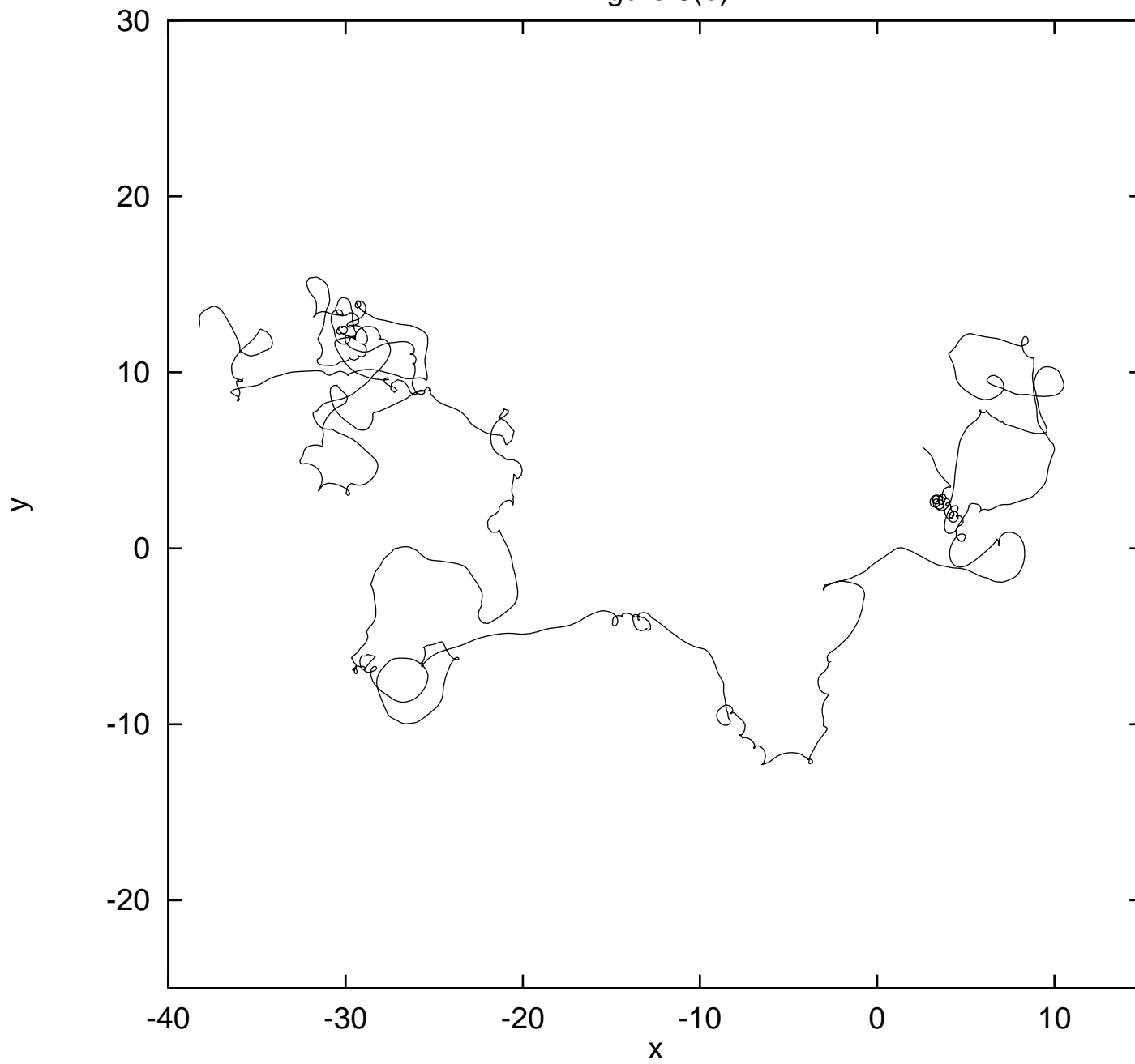


Figure 6(c)

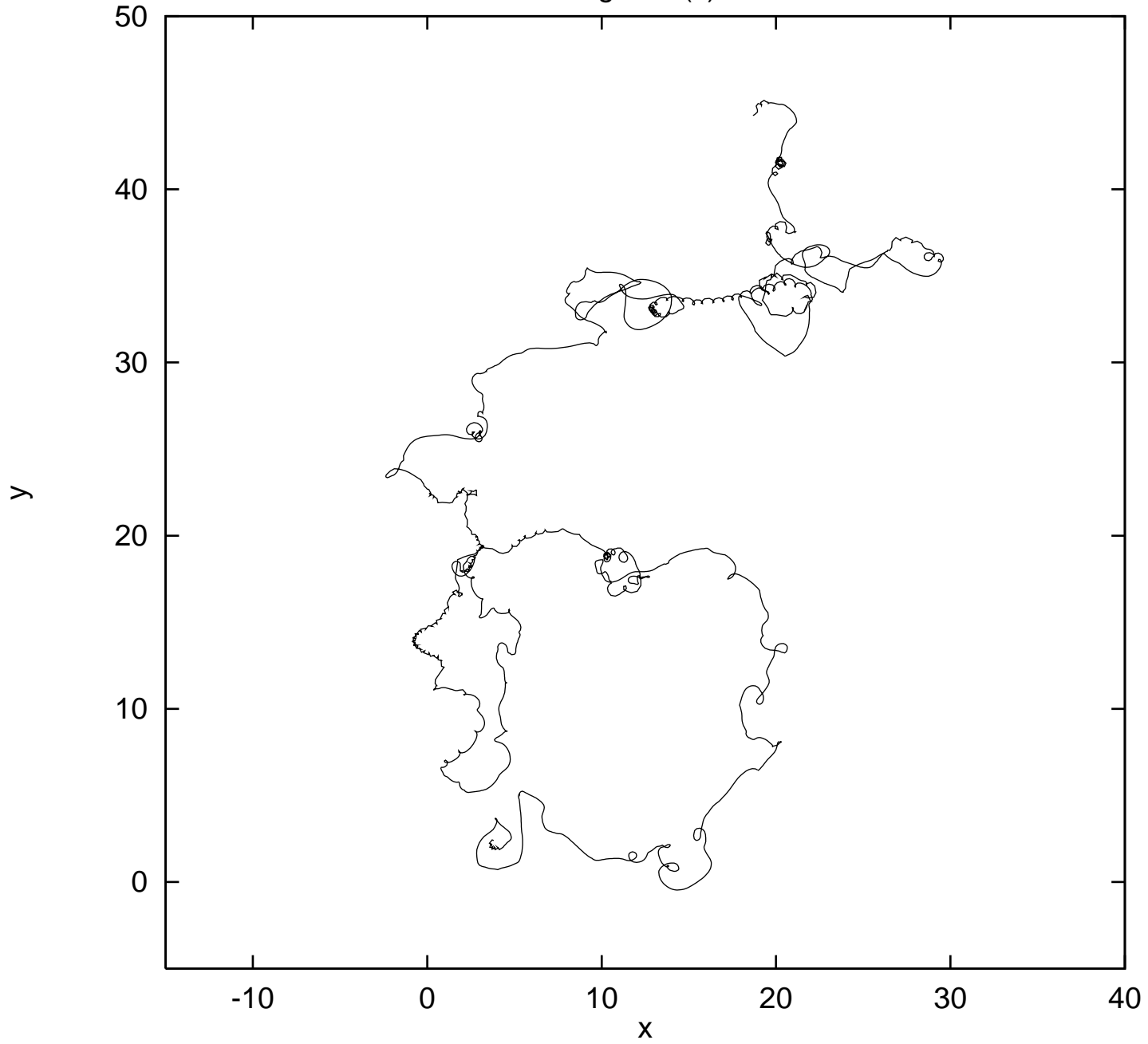


Figure 6(d)

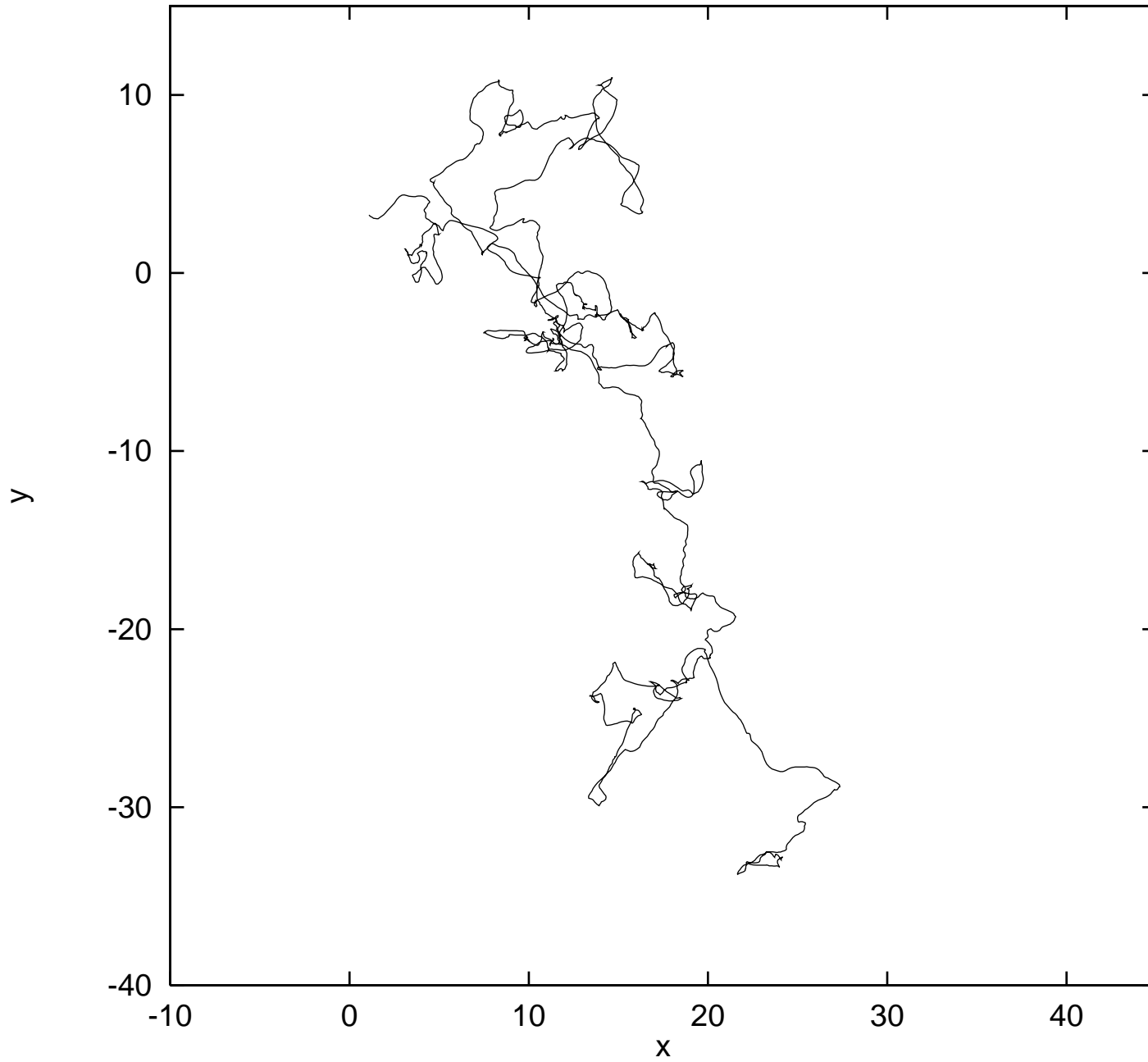


Figure 7

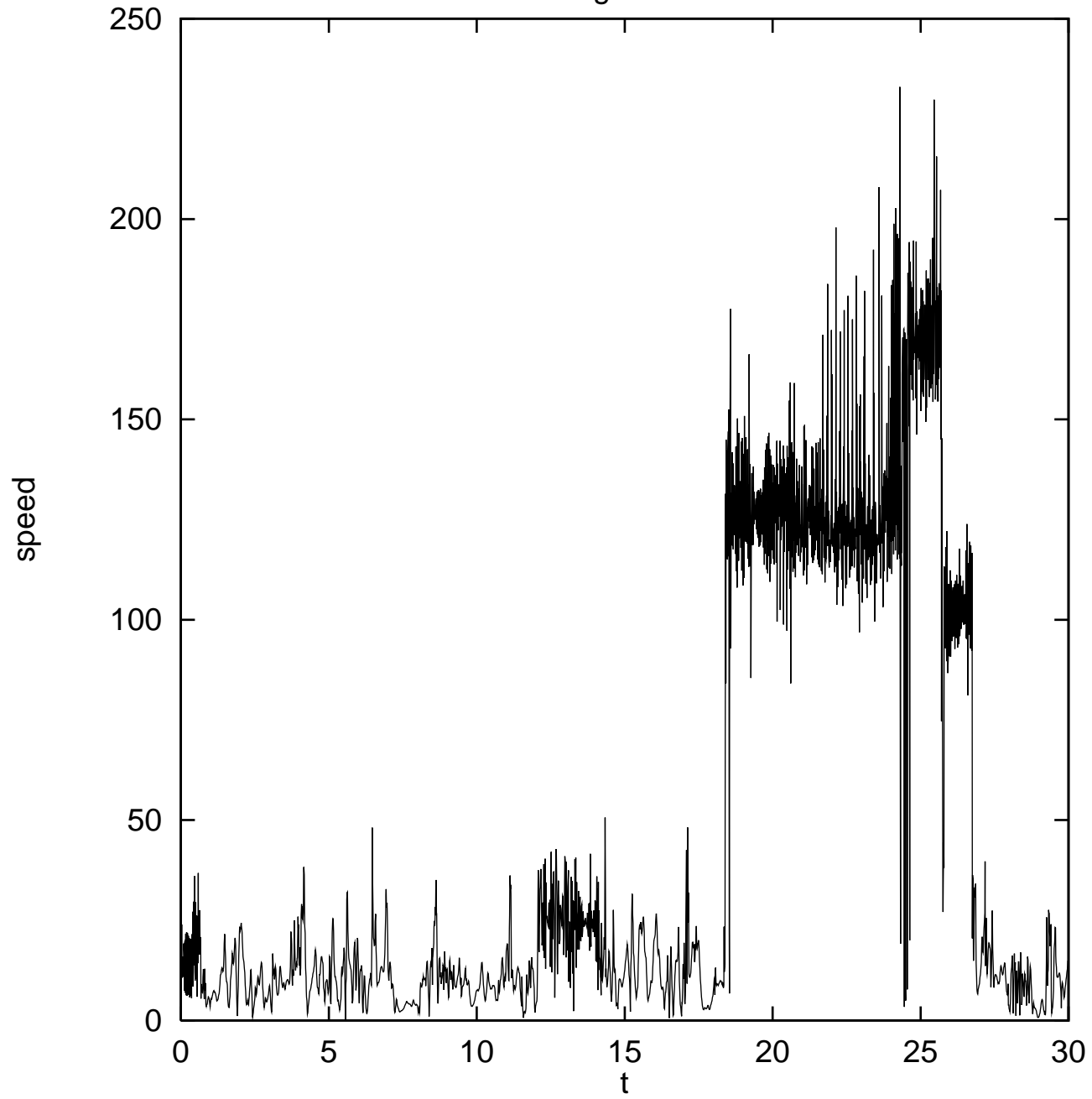


Figure 8

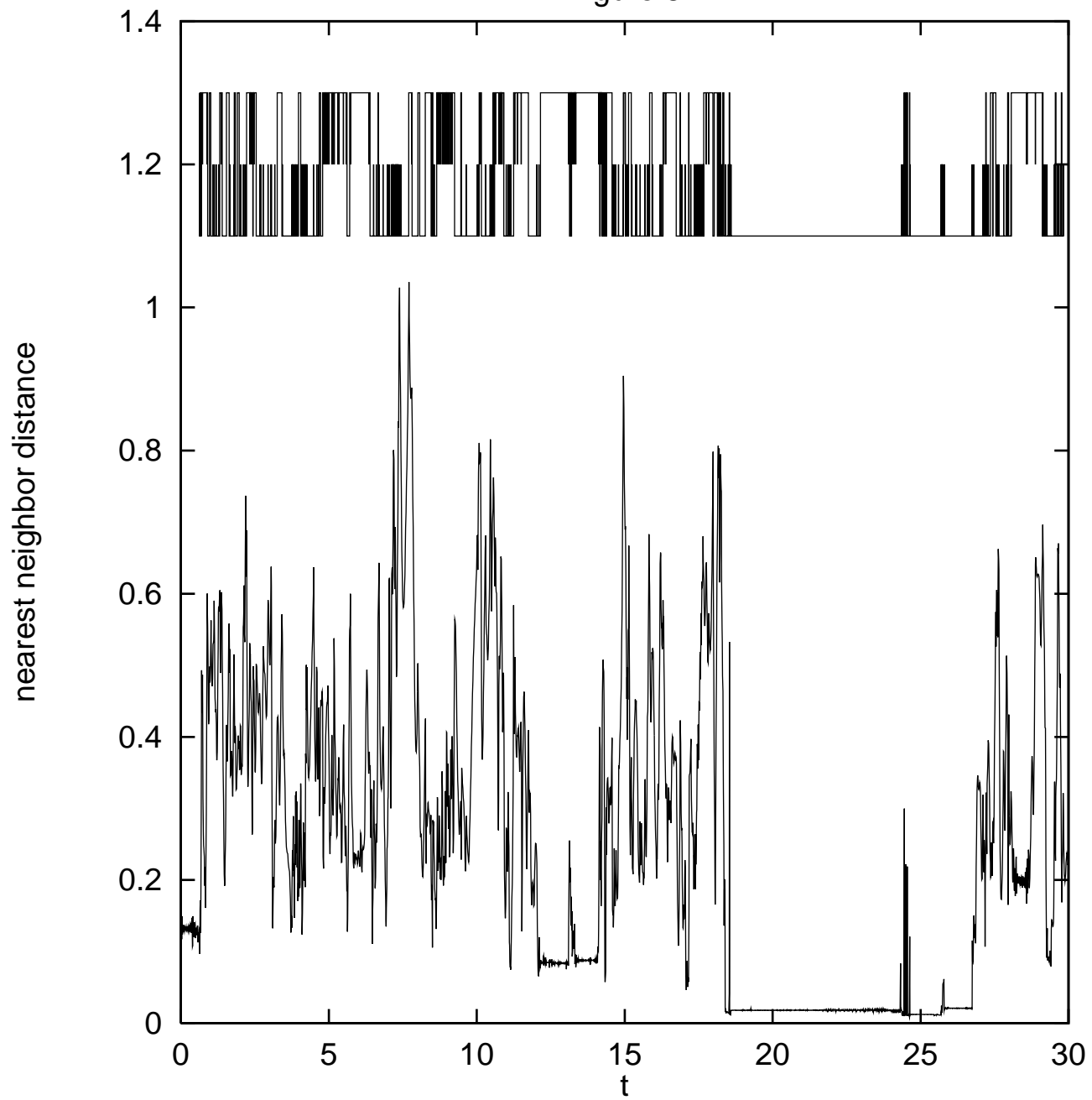


Figure 9

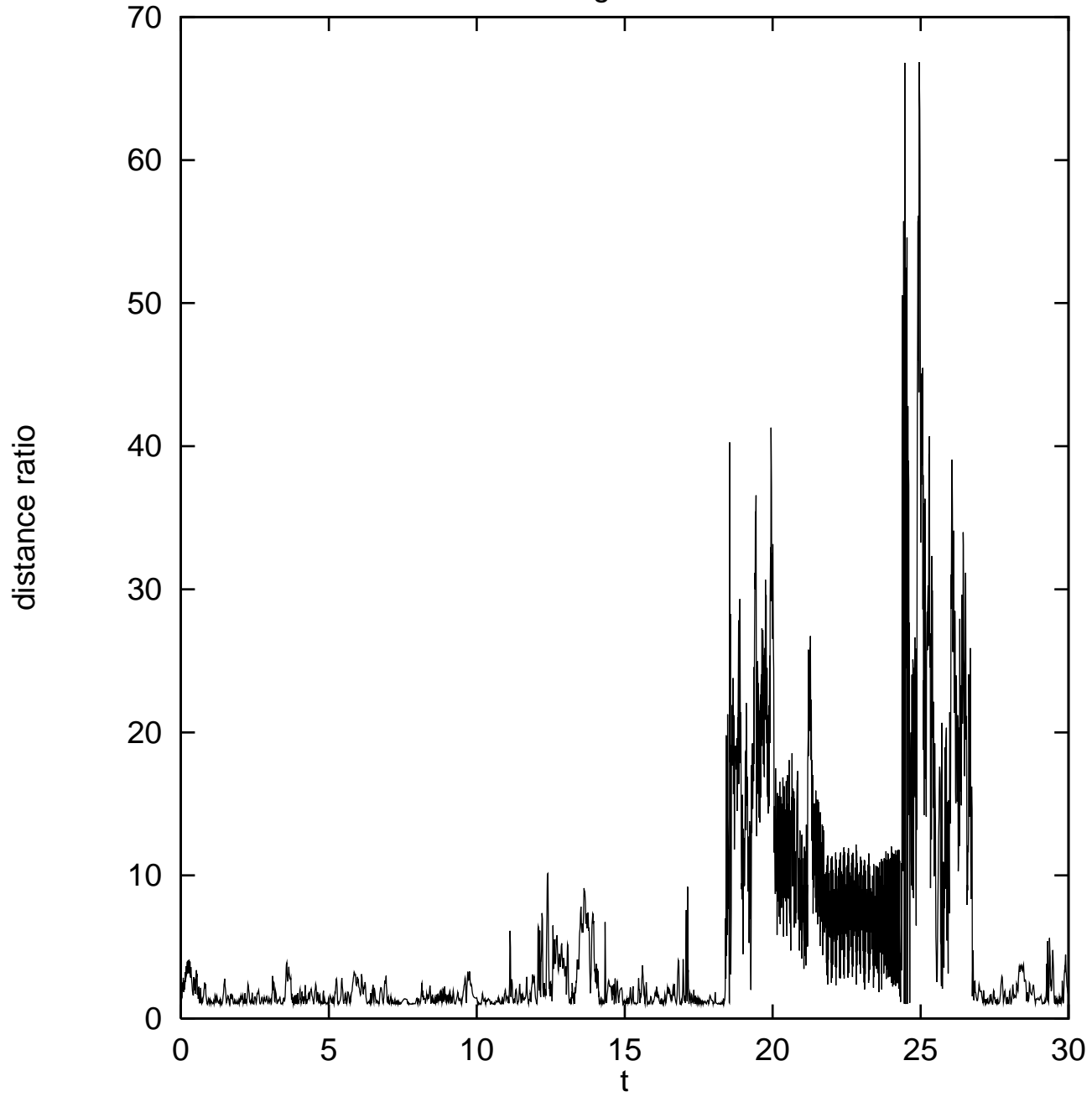


Figure 10

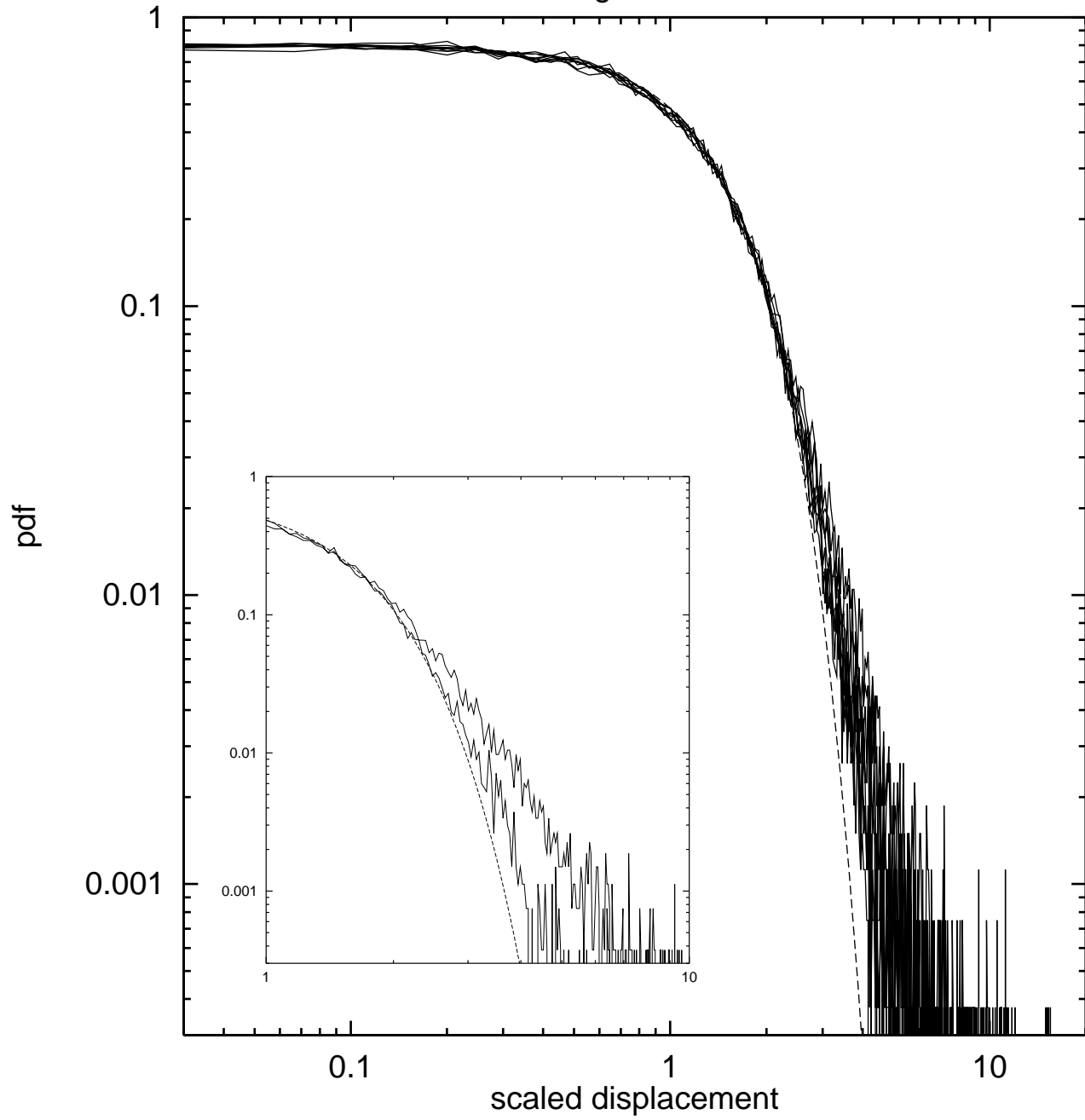


Figure 11(a)

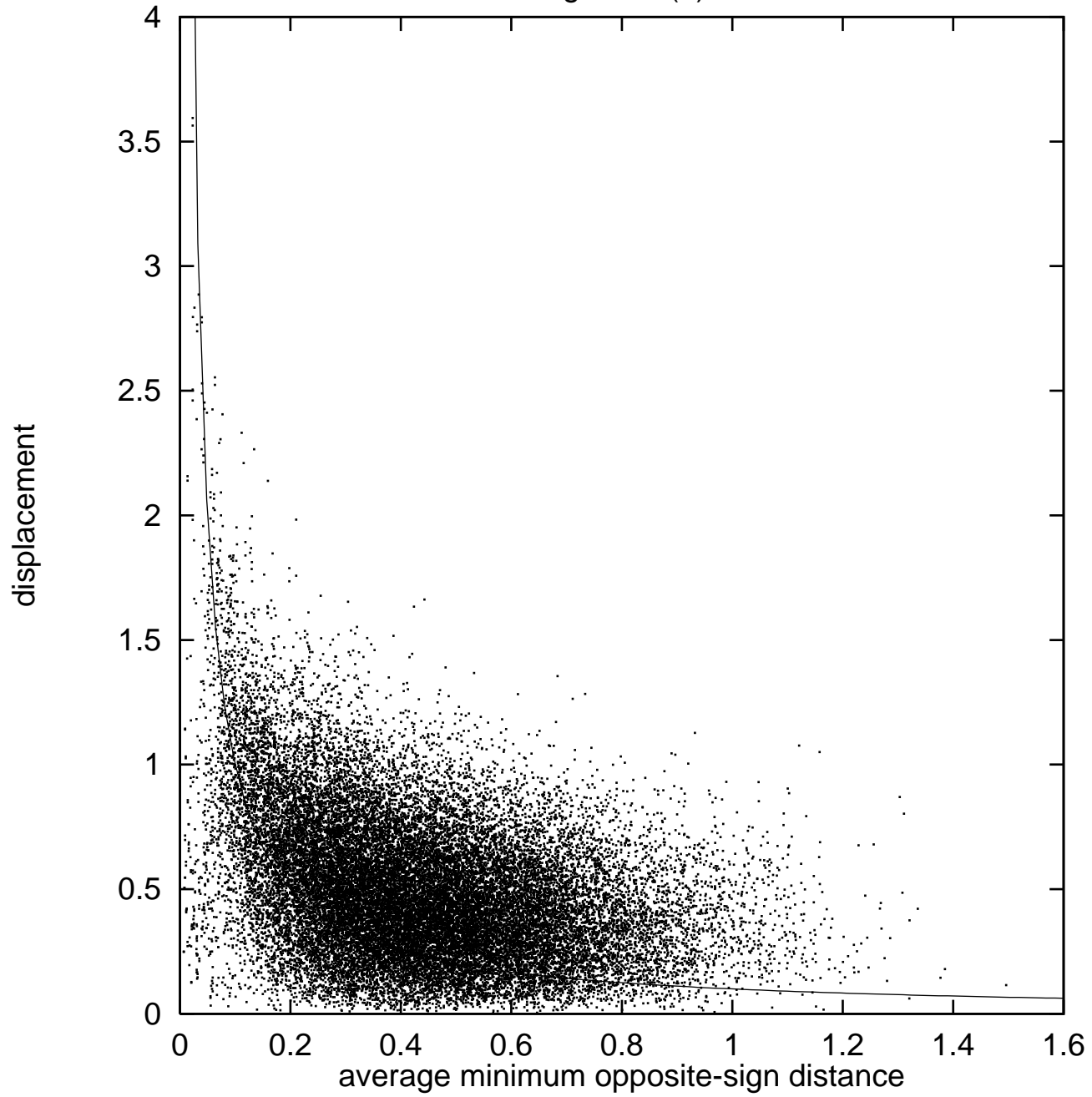


Figure 11(b)

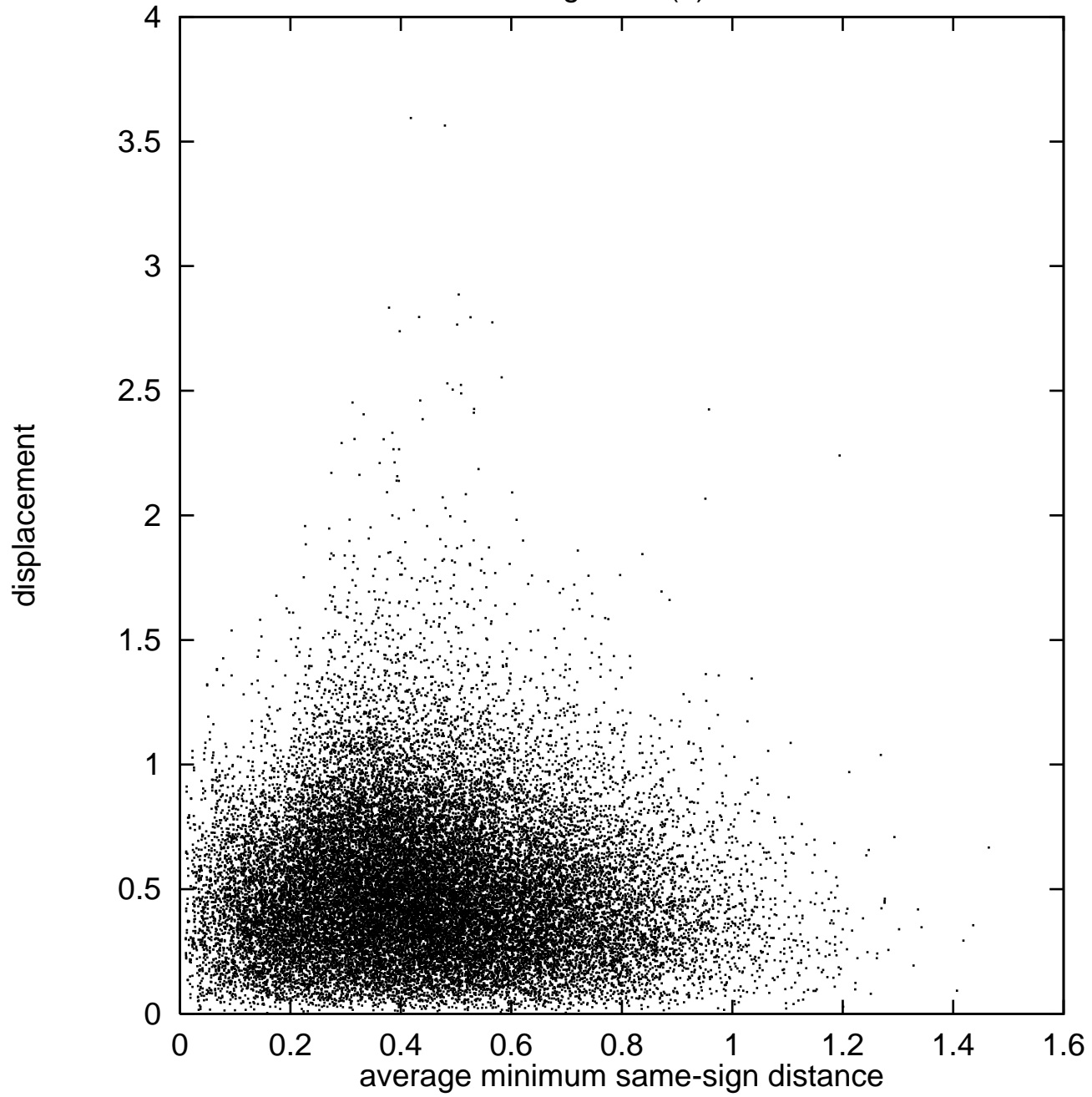


Figure 12

